ISSN 1061-933X, Colloid Journal, 2024, Vol. 86, No. 2, pp. 185–207. © Pleiades Publishing, Ltd., 2024.

Effects of pH and Indifferent Electrolyte Concentration on the Aggregate Stability of Detonation Nanodiamond Hydrosol

A. V. Volkova[a], *, A. A. Beloborodov[a], V. A. Vodolazhskii[a], E. V. Golikova[a], and L. E. Ermakova[a]

[a] *St. Petersburg State University, St. Petersburg, 199034 Russia*

**e-mail: anna.volkova@spbu.ru*

Received November 14, 2023; revised December 7, 2023; accepted December 7, 2023

Abstract—Coagulation of polydisperse detonation nanodiamond (DND) hydrosol containing primary aggregates with a prevailing average size in a range of 20–200 nm has been studied experimentally and theoretically within the framework of the classical and extended DLVO theory as depending on the concentrations of an indifferent electrolyte (NaCl) and potential-determining ions (pH). It has been shown that the surface of DND particles is charged due to the ionization of ionogenic amphoteric hydroxyl and acidic carboxyl groups located on it. The isoelectric point of the detonation nanodiamond particles has been found to correspond to pH 7.5. It has been revealed that the main stabilizing factor of the DND hydrosol is electrostatic. It has been shown that the stability and coagulation of the sol can be described within the framework of the extended DLVO theory using the effective Hamaker constant for primary porous aggregates and taking into account the initial polydispersity of the DND particles.

Keywords: detonation nanodiamond, polydisperse sol, aggregate stability, DLVO theory, effective Hamaker constant, water boundary layers, structural stabilization factor

DOI: 10.1134/S1061933X23601282

INTRODUCTION

The number of annual publications devoted to studying detonation nanodiamonds (DNDs), in which the term "nanodiamonds" is included into the list of keywords, has increased approximately 30-fold over the past twenty years. Since the beginning of the 21st century the interest in the use of DNDs for biomedical purposes [1–3] has increased due to their high biocompatibility, low cytotoxicity (the lowest among carbon nanostructures), high specific surface area, small primary particle sizes of 4–5 nm, capability of fluorescence, and the possibility of surface functionalization. DNDs are considered as a promising material to be used as a carrier for targeted delivery of biologically active and medicinal substances [4, 5], a fluorescent label [5–7], contrast agent for magnetic resonance imaging [8–11], and biosensors [12]. The emerging prospects for the successful use of DNDs in biomedicine predetermine the significance and urgency of studying aggregation processes in dilute aqueous dispersions of detonation nanodiamonds as depending on the factors that predetermine the possibility of obtaining aggregatively stable DND nanosols (composition and concentration of a background salt, pH, polydispersity of the sols, etc.), as well as their stability and functional properties when they are introduced into a body. On the other hand, nanodiamond hydrosols, as has been noted in, e.g., [13], can serve as an ideal model system for the theoretical study of the aggregation and structuring processes in dilute and concentrated nanodisperse systems, which is necessary for the development of the existing stability theories.

It should be noted that the majority of the currently available works are devoted to studying the aggregate stability of aqueous sols of either only negatively or only positively charged DND particles, i.e., the surface charge and zeta potential of which are not reversed with variations in the medium pH. Experimental and theoretical works are dealing with investigating the electrolyte-induced coagulation of sols of both primary detonation diamond nanoparticles (4–5 nm) and polydisperse sols containing mainly primary aggregates of DNDs. However, when describing the coagulation behavior of the latter type of the sols within the framework of the DLVO theory, the possible role of polydispersity in their stability and the possible difference in the values of the Hamaker constant for porous aggregates and monolithic nanoparticles are not taken into account.

The influence of the composition and concentration of an inorganic electrolyte on the stability and coagulation of diluted (solid phase content $\varphi < 0.2$ wt %) DND sols obtained from concentrated nanosols containing positively charged particles 3–4 nm in size was studied in detail elsewhere [14–17]. It has been found that the coagulation of a DND hydro-

sol that contains predominantly nanoparticle aggregates under the action of solutions of inorganic salts obeys the classical Schulze–Hardy rule and can be described from the viewpoint of the classical DLVO theory. It should be noted that, when theoretically studying the coagulation of sols with positively charged DND particles, the above works do not consider the influence of water boundary layers (BLs) on the aggregate stability of DND hydrosols.

At the same time, the study of the hydration of DNDs has been a subject of the particular interest of scientists, since, as was assumed in [18, 19], a shell of water molecules 2–4 layers thick (the thickness of the water BL on a 5-nm particle is about 10% of its size) must exist around nanoparticles of negatively charged detonation diamond. It has been shown [20, 21] that the orientation of water molecules in the first solvation layer depends on the sign of the zeta potential of particles. In contrast to positively charged DNDs, for negatively charged particles, most of the hydrogen bonds between water molecules are broken due to their electrostatic interaction with carboxyl groups. The formation of the first hydration layer near the surface of hydrogenated detonation diamond can be explained by the accumulation of excess electrons at the DND–water interface, which is stabilized by water molecules. Moreover, for positively charged particles of hydrogenated DNDs containing hydrophobic CH_x groups on their surface, the degree of hydrophilicity appears to be even higher than that for DND particles with carboxyl and hydroxyl surface functional groups. A significant difference in the structure and properties of the BLs of oppositely charged DND particles has also been noted in [22]. According to [13, 23], the interparticle distance in dilute detonation diamond hydrosols is much larger than would be expected under the action of only the ion-electrostatic repulsion forces due to the fact that the particles are interconnected through layers of water.

With regard to all of the aforementioned, despite the fact that the need to take into account the influence of water BLs on the stability and aggregation of dilute DND dispersions is obvious, the works dealing with this problem are rather scarcer to date. At the same time, they consider the contribution of the structural component to the total energy of pair interaction between particles of predominantly oxidized detonation diamond (extended DLVO theory) [24–28]. As has been shown in [26], the regularities for the coagulation thresholds of dispersions of negatively charged DND particles with an average nanoparticle aggregate size of 300 nm do not obey the Schulze–Hardy rule. Hence, the aggregate stability of DND particles is provided by not only the electrostatic factor, but also an additional factor of nanoparticle hydration. In an acidic pH region, the stability is mainly determined by structural repulsive forces, whereas, at pH 7 and above, the electrostatic factor makes the main contribution to the stability of a system. An increase in the temperature leads to a decrease in the thickness of the water BL, thereby causing coagulation of the particles [27]. It has also been shown [24, 25, 28] that the main changes caused by electrolytes in the aggregation behavior of DND hydrosols that predominantly consist of the first-kind stable aggregates are quite consistent with the data calculated in terms of the extended DLVO theory. Moreover, as noted in [29], the stability of a monodisperse DND hydrosol of negatively charged particles 4–5 nm in size may be explained from the standpoints of both the classical and extended DLVO theories, while the coagulation occurs, most likely, in the near potential minimum via the barrier mechanism. The existence of the stabilizing structural (hydration) factor is additionally confirmed by a noticeable decrease in the coagulation thresholds of the sols of positively charged DND particles upon the transition from water and protophilic (cationophilic) solvents to protophobic (cationophobic) solvents [30]. It is seen that, in most cases, it is necessary to take into account the contribution of extended water BLs to the stability of DND hydrosols when theoretically describing the aggregation processes occurring in them. This, in turn, gives rise to the problem of uncertainty in the parameters of the structural component of the pair interaction energy of DND particles.

In connection with all of the aforementioned, the goal of this work was experimental and theoretical studying the aggregate stability of a dilute polydisperse aqueous sol of DND particles as depending on the concentration of indifferent counterions at natural pH 5.8 of a salt solution (NaCl), when the sol particles are positively charged, and on the concentration of potential-determining ions (pH 4–11.5) at a constant salt background (10^{-3} M NaCl), when both the magnitude and sign of the surface charge of DND particles change with increasing pH, as well as the theoretical description of the coagulation processes in DND sols with taking into account the polydispersity of an initial hydrosol, the porosity of the primary aggregates, and the degree of the hydrophilicity of DND particle surface.

EXPERIMENTAL

The object of the study was commercial DND powder (SDTB Tekhnolog, St. Petersburg, Russia) produced by detonation of tetryl. To remove ionic impurities, the original powder was additionally purified three times by electrodialysis. For this purpose an aqueous 2.5 wt % DND dispersion was prepared. After each purification stage, the obtained dispersion was centrifuged and water was decanted. Thereafter, the sample was dried at 80°C until remaining water completely evaporated and, then, at 120°C for 2 h. The dried powder was thoroughly attrited in an agate mortar and again dispersed for 30 min in deionized water

using a RELTEK USB-7/100-TNM ultrasonic bath operating at 60 kHz for the next cleaning cycle.

Powder specific surface area S_{sp}, which was determined by the BET method measuring the thermal desorption of nitrogen with chromatographic registration, was 270 m^2/g. Average size d_o of primary nanoparticles calculated by equation

$$d_o = 6/\rho S_{sp}, \quad (1)$$

where $\rho = 3.52$ g/m^3 is the DND density, was 6.3 nm.

The phase and surface compositions of DND particles were determined by the X-ray diffraction (XRD) analysis, X-ray photoelectron spectroscopy (XPS), FTIR spectroscopy, and Raman spectroscopy.

The XRD analysis was performed in the Centre for X-ray Diffraction Studies at the Research Park, St. Petersburg State University (SPSU), using a Bruker D2 Phaser desktop automatic powder diffractometer (Bruker AXS, Germany). The phases were identified using the PDXL 2.0 software package and the Powder Diffraction File (PDF-2, 2011) powder diffraction database (Rigaku). In addition, the full-profile analysis (Rietveld method) was employed to determine the crystallite size using structural data of the Inorganic Crystal Structure Database (ICSD, 2021/2) and the TOPAS software package.

The XPS analysis of the DND powder was carried out using a Thermo Fisher Scientific Escalab 250Xi complex photoelectron and scanning Auger electron spectrometer (Thermo Fisher Scientific, United Kingdom) in the Centre for Physical Methods of Surface Investigation, SPSU.

The Raman spectrum was obtained with a Senterra instrument (Bruker, Germany) operating in the backscattering mode in the Centre for Optical and Laser Materials Research, SPSU. Raman scattering was excited using an external solid-state laser operating at a wavelength of 532 nm. The laser radiation was focused with a 20× objective (numerical aperture of 0.4), the power at the sample under the objective was 0.6 mW (2 mW at the input of the device). The spectrum was recorded within a range of 45–4400 cm^{-1}. The spectrum was measured using a diffraction grating of 400 pcs/mm, the aperture was rectangular 25 × 1000 μm. The acquisition time of a single spectrum was 150 s and the number of averagings was equal to 6.

The IR absorption spectrum was obtained by the attenuated total internal reflection (ATR) method with a Nicolet 8700 FTIR-Fourier spectrometer (Thermo Scientific, United States) equipped with an ATR attachment (Smart iTR) with a diamond crystal in the Centre for Optical and Laser Materials Research, SPSU. A deuterated triglycine sulfate (DTGS) detector was used. The resolution was 4 cm^{-1}. The presented spectrum was obtained by averaging 250 scans. The aperture was 75% of the maximum one. The Blackman–Harris function was used as an apodizing function. The phase correction was carried out using the Merz method. After subtracting the baseline caused by scattering, the spectrum was reduced to the maximum value in the region of the stretching vibrations of OH groups.

To obtain a DND hydrosol initially stable with respect to sedimentation and aggregation, an aqueous 0.25 wt % dispersion was prepared. For this purpose, purified DND powder was dispersed for 2 h in deionized water using a RELTEK USB-7/100-TNM ultrasonic bath operating at 60 kHz. The resulting suspension was allowed to settle for two weeks; then, the upper finely disperse layer was decanted and diluted with deionized water in a manner such that the optical density of the obtained sol diluted twofold was 0.18 ± 0.01 (at a light wavelength of 380 nm). The resulting sol retained its dispersity during the entire experiment (for about two months).

The particle concentration of the initial diluted DND sol and the particle size distribution were determined using the particle trajectory analysis performed with a NanoSight NS300 instrument (Malvern, United Kingdom).

The morphology and dispersity of the particles in the initial hydrosol were studied by scanning electron microscopy (SEM) using a Carl Zeiss Merlin scanning electron microscope (Carl Zeiss Merlin, Germany) in the Interdisciplinary Resource Centre for Nanotechnology at the Research Park, SPSU.

The work was devoted to studying the influence of the concentration of an indifferent electrolyte (NaCl, 5×10^{-4}–10^{-1} M) at natural pH (pH_{nat}) 5.8–6.0 and the effect of pH (4–11.5) of the sodium chloride solution with a constant concentration (10^{-3} M) on the aggregate stability of diluted DNA hydrosol. The coagulation process was studied while varying the concentrations of the indifferent electrolyte and potential-determining ions (PDIs) by the methods of turbidimetry and dynamic light scattering (DLS). The kinetic dependences of optical density D of an aqueous DND sol were obtained with a KFK-3-01 photoelectrocalorimeter in a cell 5 cm long and 2 cm wide at a wavelength of 380 nm. The measurements were carried out for 15 min. The experimental procedure has been described in detail elsewhere [31].

Particle size distributions, electrophoretic mobility values U_e, and ζ-potentials of DND particles in the initial aqueous sol, as well as in the dispersions after the end of the optical density measurements (approximately 20 min after adding the electrolyte to the sols) were determined by the DLS and laser Doppler electrophoresis methods, respectively, with a Zetasizer Nano ZS analyzer (Malvern Instruments, United Kingdom). The measurements were performed in a DTS1070 universal capillary U-shaped cell equipped with integrated gold-plated electrodes using preliminary thermostating for 2 min at 20°C. The error in determining the values of U_e was ±0.1–0.2 $m^2/(V\ s)$. From the values of the electrophoretic mobility found

experimentally within the framework of the Overbeek–Boes–Wiersema model [32] for the smallest values of electrokinetic radius κa (where κ is the Debye parameter and a is the radius of a primary nanoparticle), the values of electrokinetic potential ζ^W were calculated taking into account the polarization of the electrical double layer.

Solutions and dispersions were prepared in deionized water with specific electrical conductivity of no higher than 1.5×10^{-6} Ω^{-1} cm^{-1} (Aqualab AL Plus purification system). The required pH values were preset by adding 3×10^{-2} M and 10^{-1} M solutions of hydrochloric acid and sodium hydroxide. The pH values of the media were measured using a SevenMulti pH meter (Mettler Toledo).

Interparticle pair interaction energy V was calculated according to the classical [33–35] (Eq. (2)) and the extended [36–38] (Eq. (3)) DLVO theories to find out the nature of the observed stability and coagulation of the aqueous DND sols:

$$V = V_E + V_M, \quad (2)$$

$$V = V_E + V_M + V_S, \quad (3)$$

where V_E, V_M, and V_S are the ion-electrostatic, dispersion, and structural components of the interparticle interaction energy, respectively.

The total interparticle pair interaction energy was calculated under the assumption of the spherical shape of the particles. The energy of the ion-electrostatic interaction of identical particles was calculated for a symmetric electrolyte under the condition of a constant potential using the Oshima–Healy–White equation [39]:

$$V_E = V_E^* + \frac{4\pi a C k T}{\kappa^2}\frac{\gamma_+^4}{96} \times \left\{-\kappa h\left[1 - \tanh\left(\frac{\kappa h}{2}\right)\right] - \left[\frac{1 - \frac{\kappa h}{2}\tanh\left(\frac{\kappa h}{2}\right)}{\cosh^2\left(\frac{\kappa h}{2}\right)}\right]\right\}, \quad (4)$$

in which the expression for V_E^* has the form of

$$V_E^* = \pi a \varepsilon \varepsilon_0 \psi^2 \times \left\{\ln\left[\frac{1 + \exp(-\kappa h)}{1 - \exp(-\kappa h)}\right] + \ln\left[1 + \exp(-2\kappa h)\right]\right\}, \quad (5)$$

$$\gamma_+ = \frac{2ze\psi}{kT}, \quad (6)$$

$$\kappa = \sqrt{\frac{2z^2e^2N_AI}{\varepsilon\varepsilon_0 kT}}, \quad (7)$$

where h is the distance between particle surfaces, a is the particle radius, ε is relative dielectric constant of the solution, ε_0 is the absolute dielectric constant of vacuum, C is the electrolyte concentration in the solution, γ_+ is the dimensionless particle potential, κ is the Debye parameter, z is the multiplicity of the electrolyte counterion charge, e is the elementary charge, I is the ionic strength of the electrolyte, and ψ is the potential of the diffuse part of the electrical double layer ($\psi = \psi_d$). In the calculations, it was assumed that the ψ potential of the particles is equal to their electrokinetic potential.

The molecular component was calculated according to microscopic theory taking into account the retardation of dispersion forces [40, 41] by Eqs. (8) and (9):

$$V_M = -\frac{Aa}{12h}\left(\frac{1}{1 + 1.77p}\right) \text{ at } p < 0.5, \quad (8)$$

$$V_M = -\frac{Aa}{h}\left(\frac{2.45}{60p} - \frac{2.17}{180p^2} + \frac{0.59}{420p^3}\right) \text{ at } p > 0.5, \quad (9)$$

were $p = 2\pi h/\lambda$, λ is the characteristic wavelength of the particle material, and A is the constant of molecular (dispersion) forces (Hamaker constant). The characteristic wavelength of DND particles and the Hamaker constant were taken equal to 207 nm and 1.38×10^{-19} J, respectively [42].

The structural component of the interparticle interaction energy that results from overlapping the boundary layers at the surfaces of spherical particles was calculated using equation (10) [36, 43]:

$$V_S = \pi a K l^2 \exp(-h/l), \quad (10)$$

where K is the intensity parameter and l is the correlation length.

The curves calculated for the pair interaction energy of DND particles were used to calculate stability factors W_1 according to equation (11) for the barrier mechanism of coagulation [44–46]:

$$W_1 = \left[\int_0^\infty \frac{\beta(u)}{(u+2)^2}\exp\left(\frac{V(u)}{kT}\right)du\right] \times \left[\int_0^\infty \frac{\beta(u)}{(u+2)^2}\exp\left(\frac{V_M(u)}{kT}\right)du\right]^{-1}, \quad (11)$$

where $u = (r - 2a)/a$ is the dimensionless relative interparticle distance, r is the distance between the centers of interacting particles, a is the particle radius, and $\beta(u)$ is the hydrodynamic factor, which can be expressed as follows:

$$\beta = \frac{6u^2 + 13u + 2}{6u^2 + 4u}. \quad (12)$$

Stability factor (W_2) for the barrierless coagulation mechanism was calculated by Eq. (13) [45, 47]:

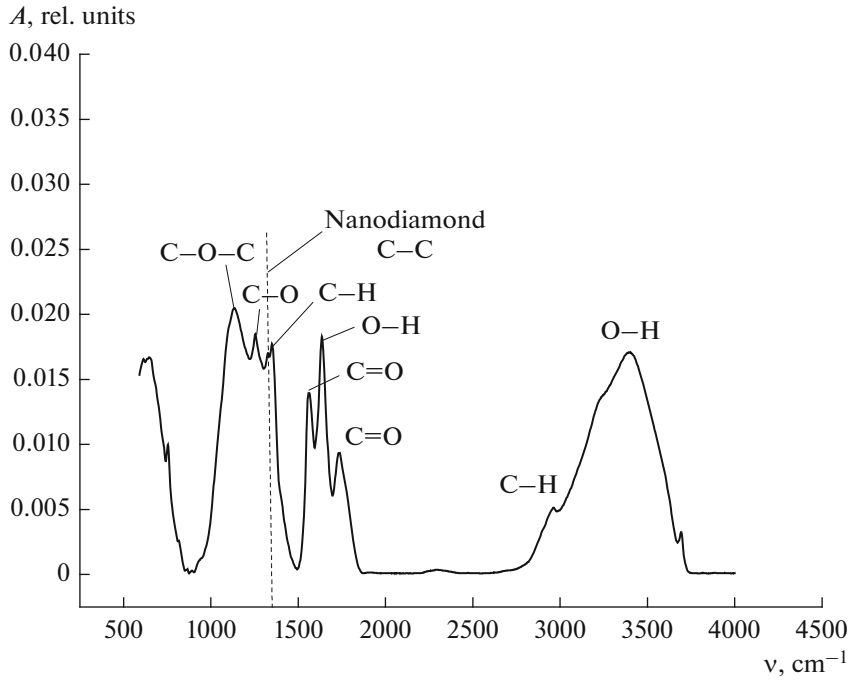

Fig. 1. IR absorption spectrum of DND powder with subtraction of the baseline and reduction to the maximum in the region of stretching vibrations of OH groups.

$$W_2 = \frac{\frac{(2a + h_{\min})}{a}\int\limits_{h_{\min}}^{\infty} \frac{\exp\left(\frac{V(u)}{kT}\right)}{(u+2)^2}du}{\left(1 - \exp\left(\frac{V_{\min}(u)}{kT}\right)\right)}, \qquad (13)$$

where W_2 is the stability factor for the barrierless coagulation in the potential minimum and $h_{\min}$ is the coordinate of the secondary potential minimum.

Total stability factor (W_{tot}) in relation to coagulation in one of the potential minima was calculated using Eqs. (14):

$$W_{\text{tot}} = \frac{W_1 W_2}{W_1 + W_2}, \text{ at } \frac{W_1}{W_2} \geq 10, \qquad (14a)$$

$$W_{\text{tot}} = \frac{2W_1 W_2}{W_1 + W_2}, \text{ at } \frac{W_1}{W_2} < 10. \qquad (14b)$$

RESULTS AND DISCUSSION

Phase Composition, Composition of Surface Groups of DND Particles, and Dispersity of Initial Hydrosol

Figure 1 shows the FTIR spectrum of purified DND powder. The intense band at 3400 cm^{-1} corresponds to the stretching vibrations of –OH groups belonging to adsorbed water and surface hydroxyl groups. The characteristic band at 1635 cm^{-1} is attributed to the bending vibrations of the –OH groups. The absorption bands at 2930 cm^{-1} and 1350 cm^{-1} are assigned to the stretching and bending vibrations of C–H bonds in alkyl CH_x groups. The band at 1730 cm^{-1} corresponds to the stretching vibrations of C=O carbonyl groups in carboxyl, ester, ketone, and aldehyde groups. The peak at 1561 cm^{-1} can be attributed to the asymmetric stretching vibrations of C=O groups in deprotonated carboxyl groups. The band with a maximum at 1251 cm^{-1} corresponds to the bending vibrations of C–O groups in epoxides and esters. The absorption band at 1125 cm^{-1} refers to the stretching vibrations of C–O bondr in C–O–C groups. The nanodiamond peak at 1325 cm^{-1} corresponds to the stretching vibrations of the C–C bonds in the DND crystal lattice [48–50].

The Raman spectroscopy (Fig. 2) and XRD analysis (Appendix, Fig. A1) data show that, in addition to the diamond phase, the studied powder contains carbon in the sp^2-hybridization corresponding to a graphite phase. As can be seen in Fig. 2, in addition to the peak at 1328 cm^{-1}, which is characteristic of nanodiamond, the spectrum exhibits a wide asymmetric peak with a maximum at 1630 cm^{-1}. According to [51], this peak is actually the superposition of the G-line of carbon in the sp^2 state, characteristic of the Raman spectrum of graphite phase-containing samples [52], and the peak corresponding to the bending vibrations of OH groups of water adsorbed on the particle surface or the functional OH groups of the surface.

The results of deconvoluting the C1*s* and O1*s* peaks in the XPS spectrum of the DND powder are shown in

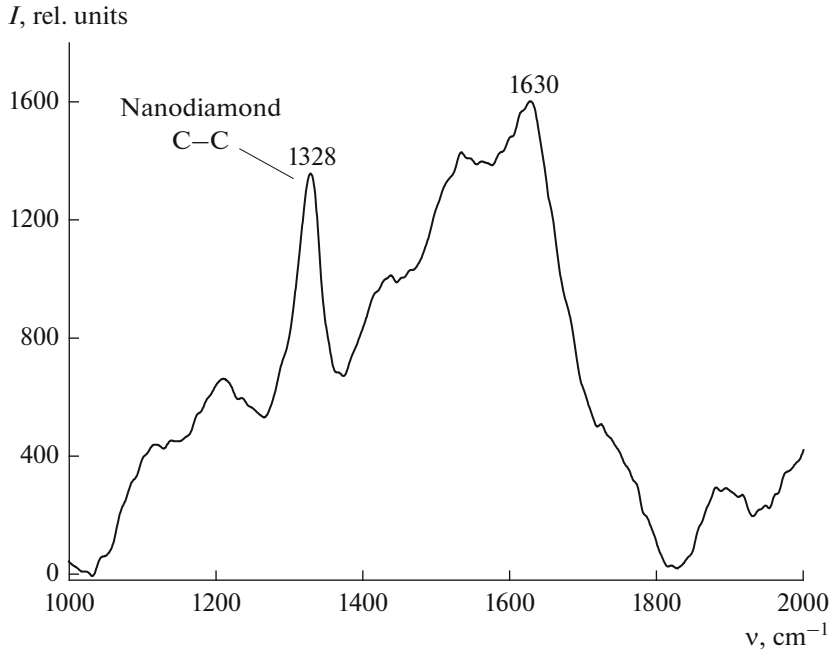

Fig. 2. Raman spectrum of DND powder.

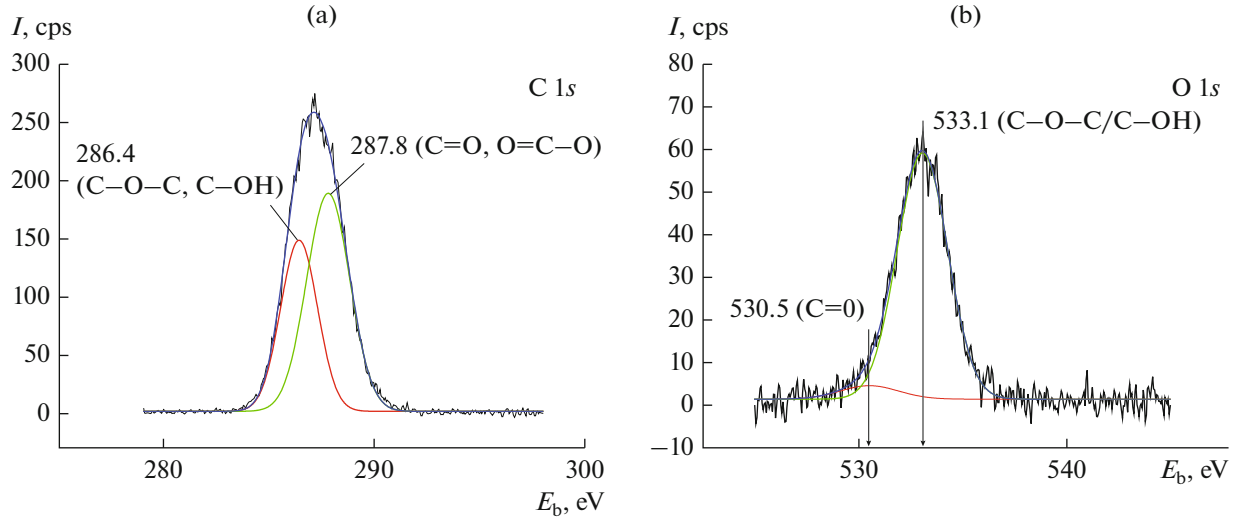

Fig. 3. (a) C1s and (b) O1*s* X-ray photoelectron spectra of DND powder.

Figs. 3a and 3b, respectively. As can be seen in Fig. 3a, the peak with a binding energy of 286.4 eV corresponds to carbon atoms at hydroxyl and in ether groups [53–57]. A binding energy of 287.8 eV is responsible for the state of carbon atoms in carbonyl [56, 57] or carboxyl groups [53, 54]. The deconvolution of the O1*s* spectrum (Fig. 3b) shows the presence of peaks with maxima at 533.1 eV (the main peak corresponding to the bond between carbon and oxygen atoms in the C–O–C and C–O–H groups) and a low-intensity peak with a maximum at 530.5 eV, which may, apparently, correspond to the binding energy of C=O bonds in carbonyl groups [55–58].

Thus, according to the XPS, FTIR, and Raman spectroscopy data, the surface of DND particles is heterogeneous and contains mainly ionogenic carboxyl and hydroxyl functional groups, as well as non-ionogenic hydrocarbon ones. The presence of ionogenic amphoteric –COH and acidic –COOH groups on the DND particle surface and their amounts and degrees of ionization determine the sign and magni-

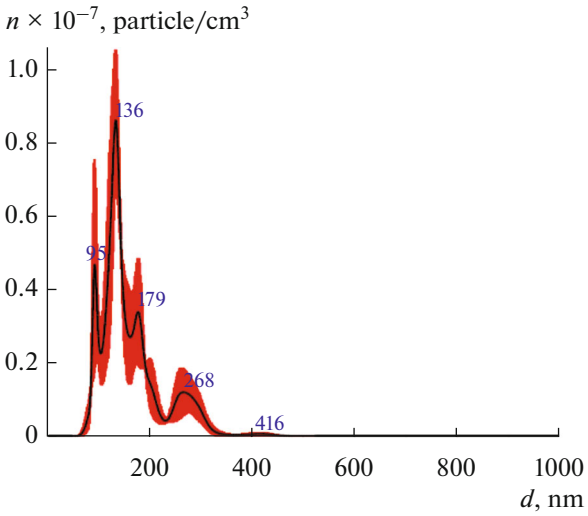

Fig. 4. Particle size distribution obtained by analyzing the particle trajectory method and averaging of three measurements for an aqueous DND sol diluted by 50 times.

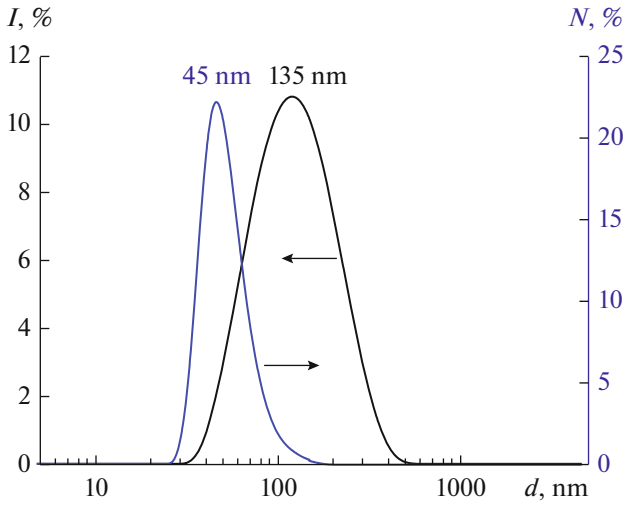

Fig. 5. Particle size distribution obtained by the DLS method for the initial aqueous DND sol.

tude of the surface charge of nanodiamond particles in a liquid dispersion medium:

$$-\mathrm{COOH} \rightleftarrows \mathrm{COO}^- + \mathrm{H}_s^+, \quad (15)$$

$$-\mathrm{COH}_2^+ \rightleftarrows -\mathrm{COH} + \mathrm{H}_s^+, \quad (16)$$

$$-\mathrm{COH} \rightleftarrows -\mathrm{CO}^- + \mathrm{H}_s^+. \quad (17)$$

Figure 4 presents the data on the particle sizes of the studied DND hydrosol stable to aggregation and sedimentation, with these data being obtained by analyzing the particle trajectories. It can be seen that the initial sol is polydisperse and contains aggregates of primary DND nanoparticles, among which particles with a size of about 135 nm prevail. The data obtained are in good agreement with the DLS results shown in Fig. 5 (average particle size d_I determined from the scattered light intensity distribution over sizes also amounted to 135 nm). The joint analysis of the SEM images of DND sol particles (Fig. 6) and the particle size distributions obtained by particle trajectory analysis and DLS methods has shown that the majority of the primary aggregates in the studied sol have sizes in a range of 20–200 nm, while their shapes are almost spherical (Fig. 6). Conventionally, this range may be divided into two parts of 70–200 and 20–70 nm, in which the most probable aggregate sizes are 135 nm and 45 nm, respectively (Fig. 5); these are average particle diameters d_N determined from the particle number size distribution. These sizes, along with the primary nanoparticle size of 6.3 nm, were used to take into account the polydispersity of the initial hydrosol when calculating the total energy of the pair interaction between DND particles. The particle concentration of the initial aqueous DND sol was $(2.8 \pm 0.9) \times 10^{10}$ particle/cm^3.

Stability of DND Hydrosol in NaCl Solutions at Natural pH

Figure 7 illustrates the results of studying the coagulation kinetics of an aqueous DND sol at natural pH (5.8–6.0) and different concentrations of sodium chloride solutions. It is seen in Fig. 7 that the studied DND sol is aggregatively stable at $C_{NaCl} \le 10^{-3}$ M, as evidenced by the constancy of the optical density during the observation for 15 min. At $C_{NaCl} \ge 10^{-2}$, the pattern of the D–t dependences is typical of fast coagulation (FC). In the intermediate concentration range, slow coagulation (SC) occurs, the rate of which increases with NaCl concentration in the solutions. More precise coagulation threshold values were determined graphically from the concentration dependences of the optical density measured for the sols 0.5 and 15 min after the addition of NaCl (Fig. 8) [31]. The values of the thresholds found in this way for the

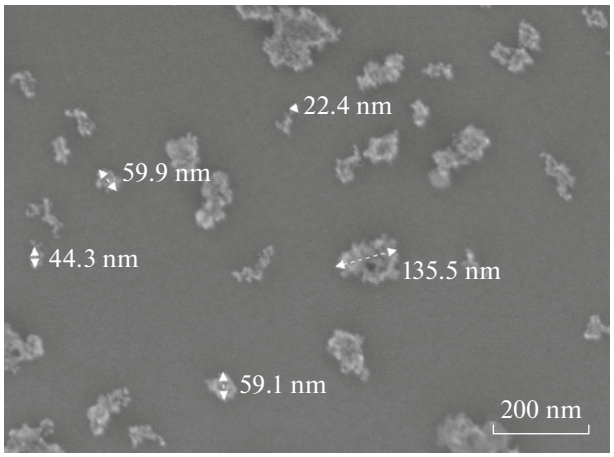

Fig. 6. SEM image of particles of the initial aqueous DND sol.

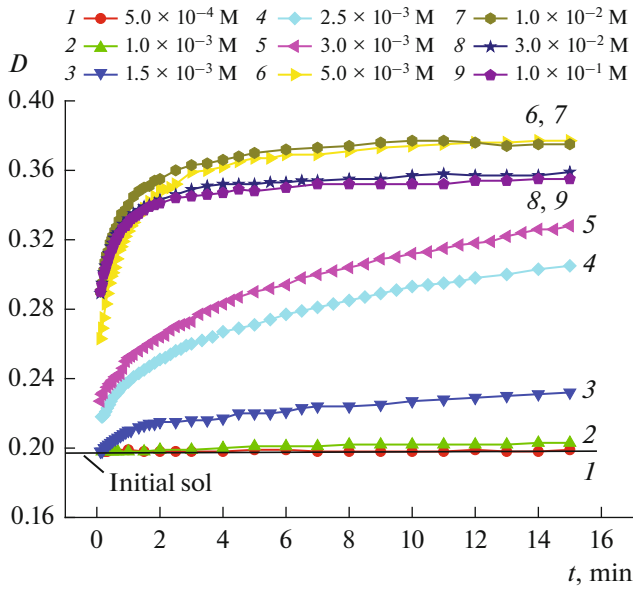

Fig. 7. Dependences of the optical density on the observation time obtained for DND hydrosols with different concentrations of sodium chloride solutions and natural pH values (5.8–6.0).

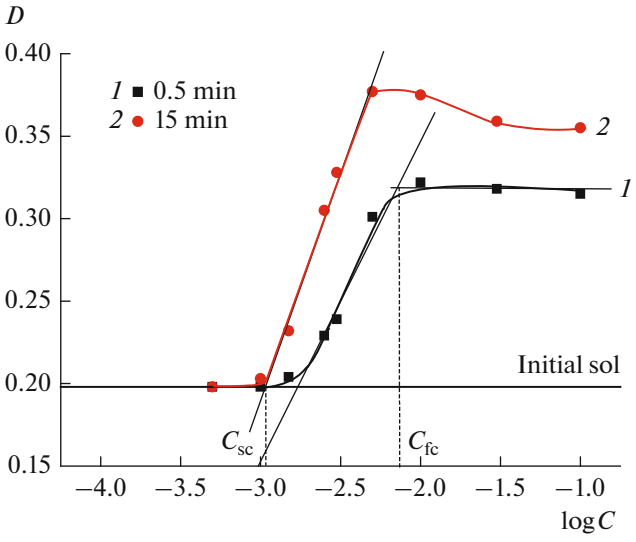

Fig. 8. Dependences of the optical density of aqueous DND sols on the concentration of NaCl solutions after (*1*) 0.5- and (*2*) 15-min observation at natural pH.

slow C_{sc} and fast C_{fc} coagulation of the DND sol were 1.1×10^{-3} M and 7.4×10^{-3} M, respectively. It should be noted that the region of slow coagulation of the sol is rather narrow, and that the obtained values of C_{fc} are noticeably lower than those for typical ion-stabilized colloids ($\sim(1–3) \times 10^{-1}$ M). This may probably be due to the relatively high value of the Hamaker constant of detonation diamond particles. It is also noteworthy that, in contrast to polydisperse sols of oxides (e.g., zirconium oxide [31]), which are distinguished by the presence of the regions of the low-intense and intense slow coagulation, the zone of the low-intense SC, in which the predominant coagulation of primary nanoparticles is expected, is atypical for the DND sols. This may probably indicate that there are actually no primary DND nanoparticles in the sol under study.

Apparently, the failure of the aggregate stability of the DND hydrosol under the influence of the indifferent electrolyte is primarily caused by a decrease in the zeta potential due to the compression of the diffuse part of the EDL with increasing NaCl concentration (Fig. 9). It should be noted that, at pH 5.8, the electrokinetic potential is positive throughout the studied concentration range. Apparently, at this pH value, the surface charge of DND particles in NaCl solutions is also positive, and the main contribution to the generation of the surface charge is made by surface reaction (16).

The calculations of the pair interaction energy of DND particles at pH_{nat} and different NaCl concentrations were carried out according to the classical and extended DLVO theories. In the latter case, when calculating the structural component of the interparticle interaction energy, correlation length parameter *l* of the structural forces was varied within a range of 1–3 nm. The calculations were performed (as indicated above) for 6.3-nm primary nanoparticles and primary aggregates 45 and 135 nm in size.

The results of calculating the pair interaction energy for primary particles are shown in Fig. 10 and in Table A1 (Appendix). It can be seen that, regardless of the calculation method, primary nanoparticles must slowly coagulate via the barrier mechanism already in a 5×10^{-4} M sodium chloride solution, and, at a NaCl concentration of 5×10^{-3} M, the fast coagulation must occur. The calculation results confirm

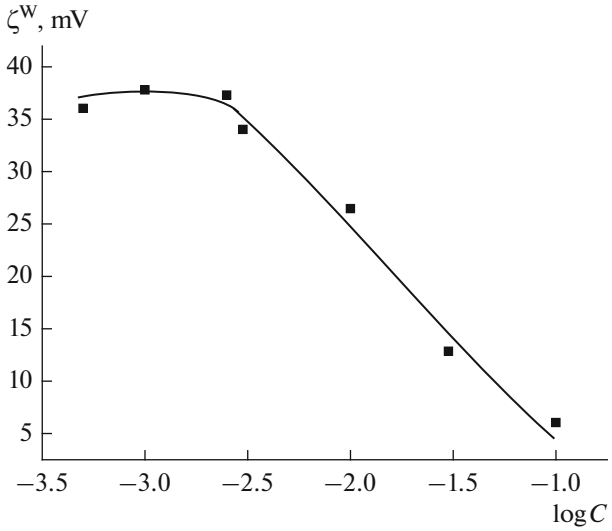

Fig. 9. Zeta potential ζ^W of DND particles as a function of the concentration of sodium chloride solution at natural pH.

the previous assumption that primary DND nanoparticles are actually absent in the studied sol. Therefore, the interaction of primary nanoparticles is not considered in the subsequent calculations.

The results of calculating the pair interaction energy for primary aggregates of DND nanoparticles according to the classical and extended DLVO theories with the Hamaker constant taken for porous aggregates corresponding to monolithic diamond particles are presented in Tables A2 and A3 (Appendix). The analysis of the obtained results has shown that, even when taking into account the structural component and varying the values of the correlation length, one cannot achieve agreement between the experimental and theoretical data. It is reasonable to assume that aggregates of DND particles have a density different from the density of monolithic nanodiamond particles. The porosity and morphology of such aggregates depend on a number of the system parameters, in particular, on the aggregate sizes; however, without going into details of the problem, it is important to note that, at this or that their structure (hardly corresponding to the densest packing of the particles), the effective Hamaker constant of the particles (i.e., A_{eff}, which really describes the forces of molecular interaction between loose aggregates) will be less than the Hamaker constant of monolithic DND particles. Therefore, in the subsequent calculations of the molecular forces for the interaction between aggregates of DND particles, several probable effective Hamaker constants were used for different degrees of looseness of random free packings of the particles ((0.58–0.86) × 10^{-19} J) (Tables A4–A7, Appendix).

The detailed comparison of the calculated and experimental data has shown that, in principle, there is a range of calculated parameters (A_{eff}, l) that makes it possible to explain the stability and coagulation of a DND sol containing particles of the two main sizes indicated above. At the same time, the smallest effective Hamaker constant of 0.58 × 10^{-19} J and correlation length l values of 1–3 nm seem to be objectively real. This is confirmed by the results presented in Figs. 11 and 12. It should be noted that, when considering the calculated data, both variations in the height of the potential barrier with variations in the NaCl concentration and the calculated values of the coagulation deceleration factors were taken into account.

The dependences of the interparticle pair interaction energy on the interparticle distance determined at different electrolyte concentrations (Fig. 11) show that the rapid coagulation threshold corresponds to the concentration range of NaCl relevant to the disappearance of the small repulsive barrier and the transition to the region of attraction between the particles at all distances between them. Figure 12 indicates that the experimental concentration dependences of the optical density (t = 0.5 min) and the average particle size (t = 20 min) are in obvious correlation with the calculated dependences of total aggregation factor

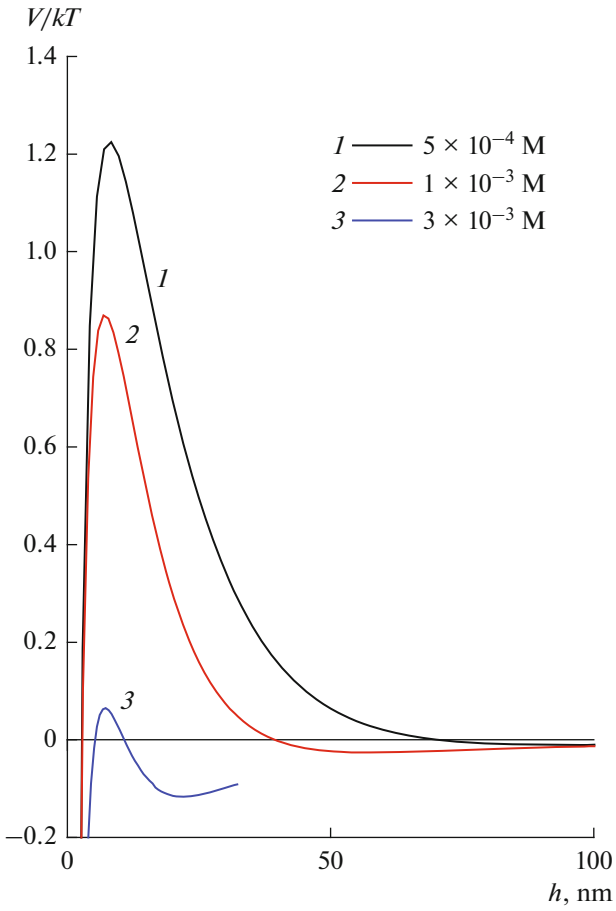

Fig. 10. Dependences of the pair interaction energy on the interparticle distance for primary DND nanoparticles (6.3 nm) at natural pH and different concentrations of sodium chloride solutions. The calculations were performed according to the extended DLFO theory. A = 1.38 × 10^{-19} J, K = 1 × 10^6 J/m^3, and l = 1.0 nm.

W_{tot}^{-1} on log C for the aforementioned group of parameters A_{eff} and l and the main sizes of the primary aggregates in the sol. It can be easily concluded that the main stabilizing factor of the DND sol is the electrostatic one. In the considered range of NaCl concentrations, coagulation of the sol for the main particle sizes may proceed via the barrier, barrierless, and mixed mechanisms. The last statement can be illustrated by, e.g., the data presented in Table 1 and Fig. 11. In this case, the main contribution to the stability of the sol is made by the primary aggregates with the smaller size (45 nm). It should be noted that, in the case of the interaction between particles of intermediate sizes, the calculation results will be only quantitatively different, while the analysis of the interparticle pair interactions will lead to the same conclusion about the nature of coagulation and quite satisfactory agreement between the theoretical and experimental data.

It is important to note that aggregates of different sizes, as well as particles of the same size, coagulate

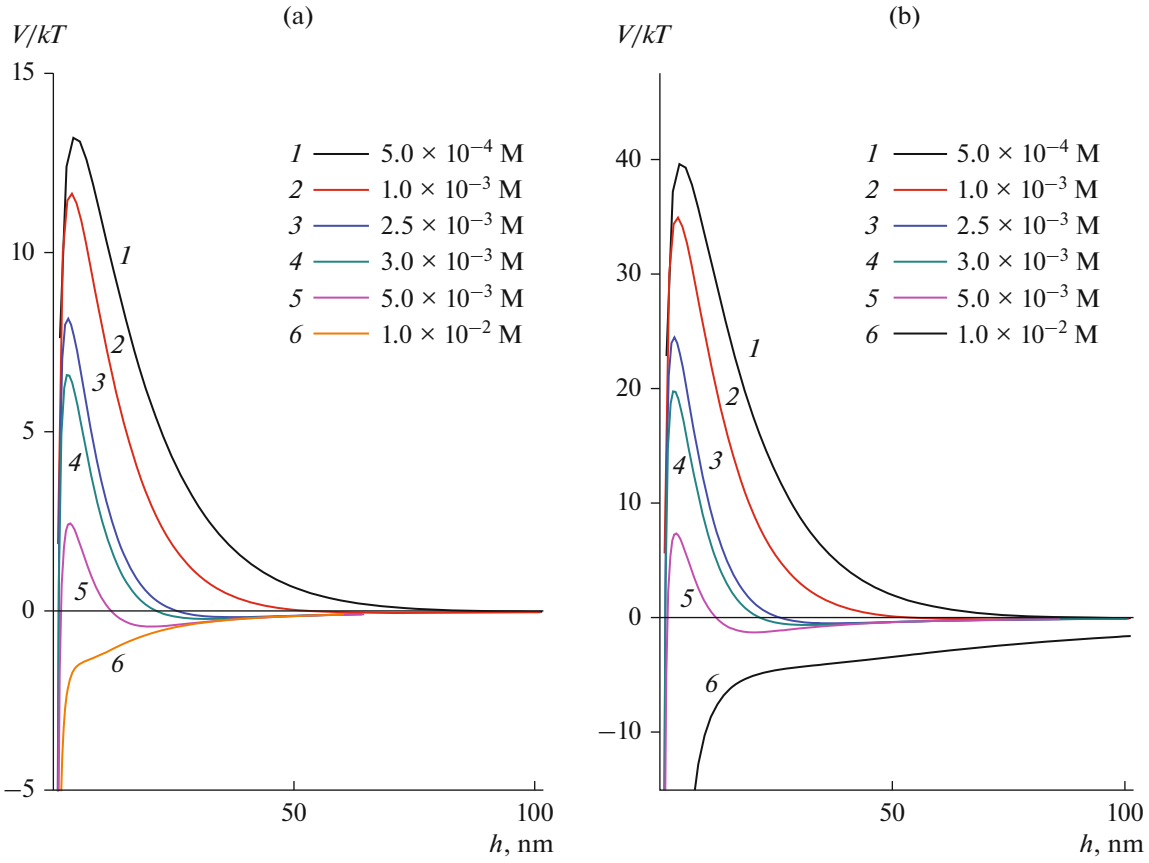

Fig. 11. Dependences of the pair interaction energy on the interparticle distance for DND aggregates ((a) 45 and (b) 135 nm) at natural pH and different concentrations of sodium chloride solutions. The calculations were performed according to the extended DLFO theory. $A_{eff} = 0.58 \times 10^{-19}$ J, $K = 1 \times 10^{6}$ J/m^3, and $l = 1.0$ nm.

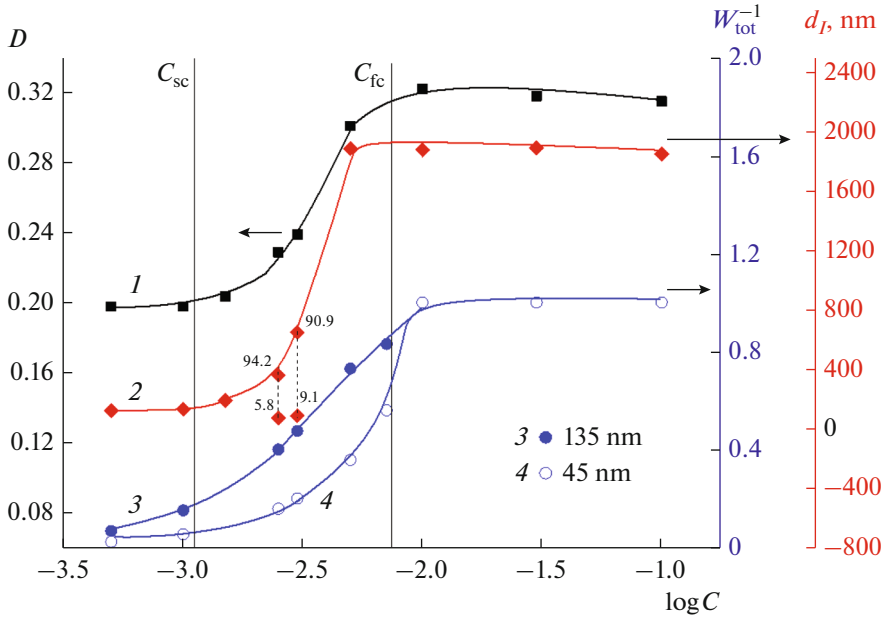

Fig. 12. Dependences of (*1*) relative optical density (t =0.5 min), (*2*) particle size (t = 20 min), and aggregation factor ($1/W_{tot}$) calculated for aggregates with sizes of (*3*) 135 and (*4*) 45 nm in DND sols on NaCl solution concentration. Calculated parameters of the structural forces are $K = 10^6$ J/m^3, $l = 1$ nm, and $A_{eff} = 0.58 \times 10^{-19}$ J. Numerical values at the points (curve *2*) are the fractions (%) of the intensity of light scattered by particles of a given size (presented for the case of the bimodal distribution).

Table 1. Some parameters of the total dependence of the pair interaction energy on the interparticle distance for DND particles (45 and 135 nm), with the parameters being calculated according to the classical and extended DLVO theories, and the aggregation factors at the natural pH value. $A_{eff} = 0.58 \times 10^{-19}$ J

C, M	Parameters V_s		V_{max}/kT	h_{max}, nm	$-V_{min}/kT$	h_{min}, nm	W_1	W_2	d, nm
	$K \times 10^6$, J/m^3	l, nm							
5×10^{-4}	1	1	13.2	4.7	0.02	115.5	2.1×10^5	43.9	45
10^{-3}			11.6	3.6	0.06	71.7	4×10^4	18.6	
2.5×10^{-3}			8.2	2.9	0.17	36.2	1.1×10^3	6.3	
3×10^{-3}			6.6	3.0	0.22	31.8	245	5.0	
5×10^{-3}			2.4	3.4	0.44	20.3	5.7*	2.8	
7×10^{-3}			0.15	4.0	0.7	13.4	1.6*	2.0	
10^{-2}			Attraction at all distances				1		
3×10^{-2}									
5×10^{-4}	0	–	13.1	4.9	0.02	115.5	1.6×10^5	43.9	45
10^{-3}			11.3	4.2	0.06	71.7	2.5×10^4	18.6	
2.5×10^{-3}			7.2	3.7	0.17	36.8	190	6.3	
3×10^{-3}			6.0	3.75	0.23	31.8	124	5.0	
5×10^{-3}			2.0	4.2	0.44	20.3	3.9*	2.8	
10^{-2}			Attraction at all distances				1		
3×10^{-2}									
5×10^{-4}	1	1	39.7	4.5	0.07	115.5	2.5×10^{16}	15.1	135
10^{-3}			35.0	3.6	0.16	71.7	2.1×10^{14}	6.6	
2.5×10^{-3}			24.5	2.9	0.52	37.2	5.4×10^9	2.5	
3×10^{-3}			19.8	3.0	0.66	31.8	5.3×10^7	2.1	
5×10^{-3}			7.34	3.4	1.3	20.3	240	1.37	
7×10^{-3}			0.45	4	2.1	13.5	1.3*	1.13	
10^{-2}			Attraction at all distances				1		
3×10^{-2}									

* At low values of the repulsive barrier (lower than 5 kT) the calculation of the stability factor by the barrier mechanism (W_1^*) is incorrect.

predominantly in the far potential minimum according to the barrierless mechanism (Table 2). Moreover, it is precisely for this process, which occurs at a higher rate than the coagulation of particles of the same size and, therefore, has a greater effect on the stability of the polydisperse sol, that the calculated parameters best correspond to the experimental data.

Stability of Aqueous DND Sols at Different PDI Concentrations (pH).

The results of studying the coagulation kinetics of an aqueous DND sol at different pH values of a 10^{-3} M sodium chloride solution by the turbidimetry method are presented in Fig. 13. It can be seen that, as the pH decreases from its natural value of 5.8, the dispersion remains aggregatively stable. At pH > pH_{nat}, the dispersions coagulate. The pattern of the curves indicates that, at pH 6.61 and 11.5, the slow coagulation occurs, while, at pH 11.5, it is more intense, and, at pH 8.66, fast coagulation occurs. Figure 14 shows that the isoelectric point (IEP) of DND particles takes place at pH 7.5. Therefore, at pH < 7.5, the sol particles are positively charged, while, at pH > 7.5, they are negatively charged (assuming that NaCl is indifferent). In this case, the positive surface charge of DND at pH < 7.5 is apparently due to the protonation of the surface hydroxyl groups.

Table 2. Some parameters of the total dependence of the pair interaction energy on the interparticle distance for different-sized DND particles (45 and 135 nm), with the parameters being calculated according to the extended DLVO theory, and aggregation factors at the natural pH value. $A_{eff} = 0.58 \times 10^{-19}$ J

C, M	Parameters V_s		V_{max}/kT	h_{max}, nm	$-V_{min}/kT$	h_{min}, nm	W_1	W_2	ζ^w, mV
	$K \times 10^6$, J/m^3	l, nm							
5×10^{-4}	1	1	19.7	4.4	0.03	113.5	6.7×10^7	28.5	37.2
10^{-3}			17.5	3.6	0.08	71.7	6.6×10^6	12.6	37.5
2.5×10^{-3}			12.2	2.9	0.26	37.2	3.2×10^4	4.4	36.5
3×10^{-3}			9.9	3.0	0.33	31.8	3.2×10^3	3.5	35.2
5×10^{-3}			7.2	2.84	0.59	22.2	142	2.25	30.9
10^{-2}			Attraction at all distances				1		24.8
3×10^{-2}									14.5

As can be seen in Fig. 15, the results of determining the optical density of the sol and the average particle size as depending on pH at a constant observation time are in good agreement with each other. At the same time, attention is drawn to the fact that both, in the region of stability and in the case of the most intense coagulation (at pH 8.66 and 11.5), the particle distribution is bimodal due to the polydispersity of the initial DND sol. As can be seen in Fig. 16, the sol stable in a 10^{-3} M sodium chloride solution at natural pH 5.8 is characterized by two most probable particle sizes equal to 135 and 24 nm (d_I) or 24 and 60 nm (d_N). The fact that, when studying the stability of the sol in a 10^{-3} M sodium chloride solution at pH 5.8, only one peak corresponding to rather large DND aggregates 135 nm in size is observed can be explained by the peculiarities inherent in the DLS method, when it is used to study polydisperse samples containing both large and small particles. It should be noted that the comparison between the obtained data and the SEM results (Fig. 6) shows that the main fraction of sol particles has, apparently, size $d \le 60$ nm, while not all particles are "visible" by the particle trajectory analysis. Accordingly, the determined particle concentration of the sol may be underestimated. This assumption is in good agreement with the results of studying the stability at pH 5.8 (Fig. 12). Provided that the main contribution to the stability of the sol is made by particles with an average size of less than 60 nm, the coagulation of larger particles (at least in the initial region of slow coagulation) against the background of maintaining the dispersity of particles with a relatively small size may have no significant effect on the observed overall picture of the stability of the DND sol. Because of the aforementioned, particles with sizes of 24 and 60 nm were also taken into account in subsequent calculations.

The potential energy of the pair interaction between the particles of the DND sols, which was calculated as a function of the interparticle distance, and the corresponding factors of the sol stability for the bar-

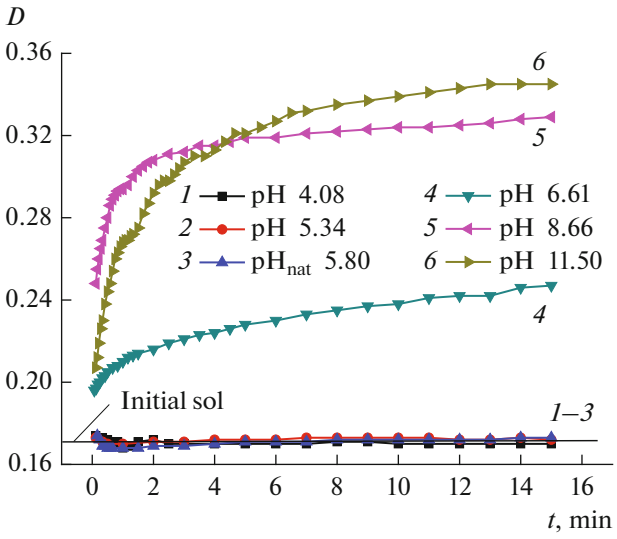

Fig. 13. Time dependences of optical density at different pH values of a 10^{-3} M sodium chloride solution.

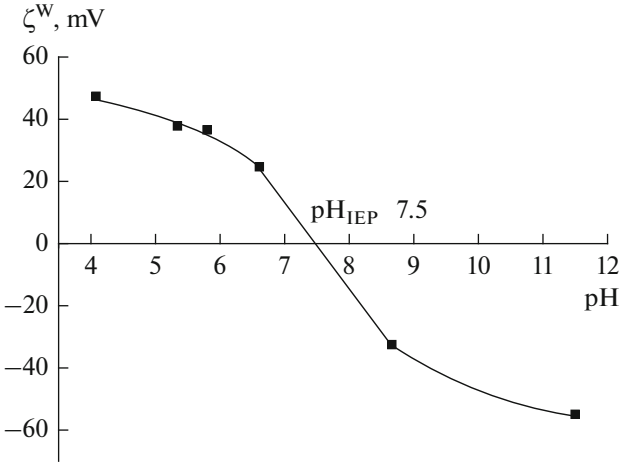

Fig. 14. Dependences of electrokinetic potential ζ^w on the pH of a 10^{-3} M sodium chloride solution for DND hydrosol particles.

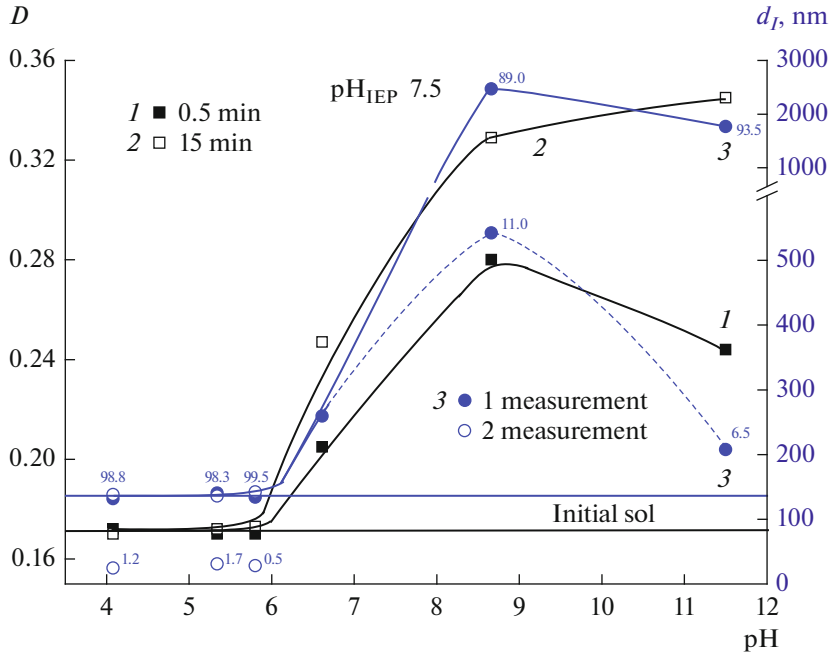

Fig. 15. Dependences of the optical density of aqueous DND sols on NaCl solution concentration after (*1*) 0.5- and (*2*) 15-min observations, as well as (*3*) the dependence of average particle size (t = 20 min), at natural pH. Numerical values at the points (curve 3) denote the fractions (%) of the intensity of light scattered by particles of a given size (presented for the case of a bimodal distribution).

rier and the barrierless mechanisms are given in Tables 3 and 4. In this case, the same calculated parameters A_{eff} and l were employed as those used when plotting the $V(h)$ curves in Fig. 4. When considering the calculated data, we took into account both variation in the height of the potential barrier with variations in pH (in the case of a barrier value of less than 5 kT) and the calculated values of coagulation deceleration factors. Note that the calculated values of stability factor W_1 for relatively low particle repulsion barriers (data in the tables are presented in italics) do not agree satisfactorily with the results of studying the stability of the sol.

It can be seen in Table 3 that, for positively charged DND particles with a size of 45 nm in a pH range of 4.1–5.8, stability and rather slow coagulation via the barrier mechanism at pH 6.6 are predicted; a similar prediction is valid for DND particles with a size of 60 nm (Table 4). For larger particles (135 nm), the slow coagulation is predicted to occur predominantly by the barrierless mechanism in a pH range of 4.1–6.6; for small particles with a size of 24 nm, the slow coagulation is predicted to proceed predominantly by a barrier mechanism in a pH range of 5.8–6.6. For negatively charged DND particles, both slow and fast coagulation, as well as the sol stability, may be expected depending on the particle size and pH (Tables 3, 4). The same conclusion may be made when considering the pair interaction for particles of different sizes (Tables 5, 6).

In general, we may talk about a qualitative correspondence between the turbidimetry data and the calculated $V(h)$ dependencies. Most probably, the incomplete correlation between the theoretical calculations and the experimental results for different pH values (first of all, only for pH 8.66) is due to the fact that the BLs of water near the DND particle surfaces are rather sensitive to the concentration of PDIs; the use of constant parameters of the structural component in the calculations is a significant approximation.

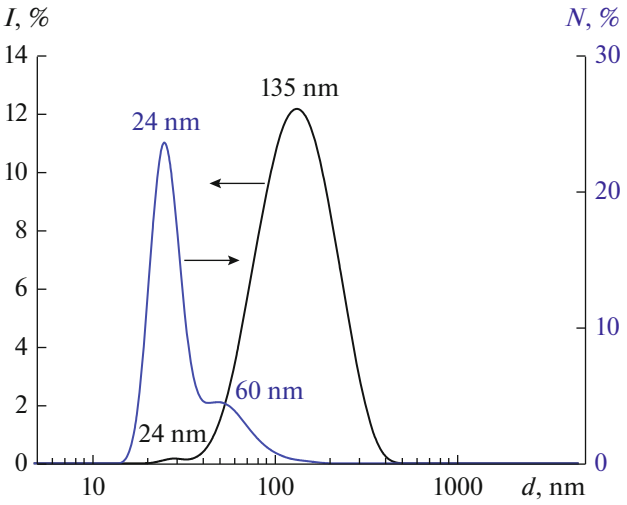

Fig. 16. Particle size distribution obtained by the DLS method for a DND sol in a 10^{-3} M NaCl solution at pH 5.8.

Table 3. Some parameters of the total dependence of the pair interaction energy of DND on interparticle distance for aggregates (45 and 135 nm), with the parameters being calculated according to the extended DLVO theory, and aggregation factors at different pH values of a 10^{-3} M sodium chloride solution. $A_{eff} = 0.58 \times 10^{-19}$ J

pH	Parameters V_s		V_{max}/kT	h_{max}, nm	$-V_{min}/kT$	h_{min}, nm	W_1	W_2	ζ^w, mV	d, nm
	$K \times 10^6$, J/m^3	l, nm								
4.08(+)	1	1	64.0	2.503	0.16	73.2	$>10^{26}$	6.6	47.4	135
5.34(+)			35.3	3.5	0.18	69.2	$>10^{14}$	6.23	37.8	
5.8(+)			27.8	4.1	0.19	66.9	1.7×10^{11}	5.9	34.8	
6.6(+)			9.2	6.8	0.22	59.60	1.8×10^3	5.0	24.7	
8.66(–)			22.6	4.5	0.19	65.1	10^9	5.6	–32.5	
11.5(–)			34.8	1.2	4.5	8.6	10^{13}	1.0	–54.9	
4.08(+)	1	1	21.3	2.5	0.05	73.0	4.8×10^8	18.9	47.4	45
5.34(+)			11.8	3.5	0.06	69.2	4.3×10^4	17.5	37.8	
5.8(+)			9.2	4.1	0.06	66.9	3.7×10^3	16.6	34.8	
6.6(+)			3.2	6.8	0.07	59. 0	11.7	14.0	24.7	
8.66(–)			7.5	4.5	0.06	65.1	737	15.9	–32.5	
11.5(–)			11.6	1.2	1.5	8.6	7.7×10^3	1.3	–54.9	

Table 4. Some parameters of the total dependence of the pair interaction energy on the interparticle distance for DND aggregates (24 and 60 nm), with the parameters being calculated according to the extended DLVO theory, and aggregation factors at different pH values of a 10^{-3} M sodium chloride solution. $A_{eff} = 0.58 \times 10^{-19}$ J

pH	Parameters V_s		V_{max}/kT	h_{max}, nm	$-V_{min}/kT$	h_{min}, nm	W_1	W_2	ζ^w, mV	W_Σ	d, nm
	$K \times 10^6$, J/m^3	l, nm									
4.08(+)	1	1	11.4	2.5	0.036	73.0	3.9×10^4	34.9	47.4	34.9	24
5.34(+)			6.3	3.5	0.03	69.2	303	32.3	37.8	58.4	
5.8(+)			4.9	4.1	0.033	66.9	87	16.6	34.8	27.9	
6.6 (+)			1.6	6.8	0.04	59. 0	4.7	25.9	24.7	7.9	
8.66(–)			4.0	4.5	0.035	65.1	65.1	29.4	32.5	40.5	
11.5(–)			6.2	1.2	0.8	53.8	120	1.8	54.9	1.8	
4.08(+)	1	1	28.4	2.503	0.076	73.0	4.6×10^{11}	14.3	47.4	14.3	60
5.34(+)			15.7	3.5	0.08	69.2	1.7×10^6	13.2	37.8	13.2	
5.8(+)			12.3	4.1	0.08	66.9	6.6×10^4	12.6	34.8	12.6	
6.6(+)			4.1	6.8	0.1	59. 0	24.3	10.6	24.7	14.8	
8.66(–)			10.6	4.5	0.09	65.1	7×10^3	12.1	32.5	12.1	
11.5(–)			15.5	1.2	2.0	8.6	6×10^5	1.15	54.9	1.15	

CONCLUSIONS

The spectroscopic study of the composition of surface functional groups has shown that the DND particle surface is heterogeneous. It mainly contains ionogenic carboxyl and hydroxyl functional groups, as well as nonionogenic hydrocarbon ones. Particle surface is charged due to the ionization of ionogenic amphoteric –COH and acidic –COOH groups on the DND surface.

Table 5. Some parameters of the total dependence of the pair interaction energy on the interparticle distance for DND aggregates of different sizes (24 and 60 nm), with the parameters being calculated according to the extended DLVO theory, and aggregation factors at different pH values of a 10^{-3} M sodium chloride solution. $A_{eff} = 0.58 \times 10^{-19}$ J

pH	Parameters V_s		V_{max}/kT	h_{max}, nm	$-V_{min}/kT$	h_{min}, nm	W_1	W_2	ζ^W, mV	W_Σ
	$K \times 10^6$, J/m^3	l, nm								
4.08(+)	1	1	16.3	2.5	0.04	73.0	4.8×10^6	24.6	47.4	24.6
5.34(+)			9.0	3.5	0.04	69.2	4.2×10^3	22.8	37.8	22.6
5.8(+)			7.0	4.1	0.05	66.9	679	21.6	34.8	20.9
6.6(+)			2.25	6.7	0.22	56.5	8.0	17	24.7	11.3
8.66(–)	1	1	5.9	4.6	0.05	67.7	216	22.2	32.5	40.2
11.5(–)			8.8	1.2	1.15	8.6	1.6×10^3	1.46	54.9	1.46

Table 6. Some parameters of the total dependence of the pair interaction energy on the interparticle distance for DND aggregates of different sizes (24 and 135 nm), with the parameters being calculated according to the extended DLVO theory, and aggregation factors at different pH values of a 10^{-3} M sodium chloride solution. $A_{eff} = 0.58 \times 10^{-19}$ J

pH	Parameters V_s		V_{max}/kT	h_{max}, nm	$-V_{min}/kT$	h_{min}, nm	W_1	W_2	ζ^W, mV	W_Σ
	$K \times 10^6$, J/m^3	l, nm								
4.08(+)	1	1	20.0	2.5	0.05	73.0	7.3×10^7	20.1	47.4	20.1
5.34(+)			9.0	3.5	0.04	69.2	4.2×10^3	22.8	37.8	22.8
5.8(+)			11	3.5	0.06	69.2	1.2×10^4	18.6	34.8	18.6
6.6(+)			2.9	6.8	0.07	59	5.9	14.9	24.7	8.6
8.66(–)	1	1	7.0	4.4	0.06	65.1	257	16.9	32.5	31.7
11.5(–)			10.9	1.2	1.4	8.6	4.7×10^3	1.3	54.9	1.3

The aggregate stability and electrokinetic properties of a polydisperse aqueous sol of detonation nanodiamond with a particle concentration of $(2.8 \pm 0.9) \times 10^{10}$ particle/cm^3 have been studied at natural pH values (5.8–6.0) and different concentrations of solutions of indifferent electrolyte, NaCl, as well as different pH values in a 10^{-3} M sodium chloride solution. The pH value of the IEP of DND particles has been determined to be 7.5. The thresholds found for the slow and fast coagulation of a sol of positively charged DND particles at pH 5.8 have appeared to be 1.1×10^{-3} M and 7.4×10^{-3} M, respectively. It has been shown that the studied DND hydrosol is characterized by a very narrow region of slow coagulation, and the C_{fc} value noticeably lower than that for typical ion-stabilized colloids. This fact may be due to the relatively high value of the Hamaker constant for detonation diamond particles.

It has been revealed that the coagulation of DND hydrosols is caused mainly by a decrease in the contribution of the ion-electrostatic component of the interparticle pair interaction energy due to a reduction in the absolute value of the zeta potential with increasing concentration of NaCl solutions or when approaching the IEP.

The combined analysis of the experimental and theoretical results has shown that there are practically no primary DND nanoparticles in the studied sol, and the main contribution to the stability is made by DND nanoparticle aggregates with an average size of about 60 nm or less. The region of calculated parameters A_{eff} and l, which makes it possible to explain the stability and coagulation of a DND sol containing particles of several main sizes has been determined within the framework of the extended DLVO theory.

APPENDIX

EFFECTS OF pH AND INDIFFERENT ELECTROLYTE CONCENTRATION ON AGGREGATE STABILITY OF AQUEOUS DND SOL

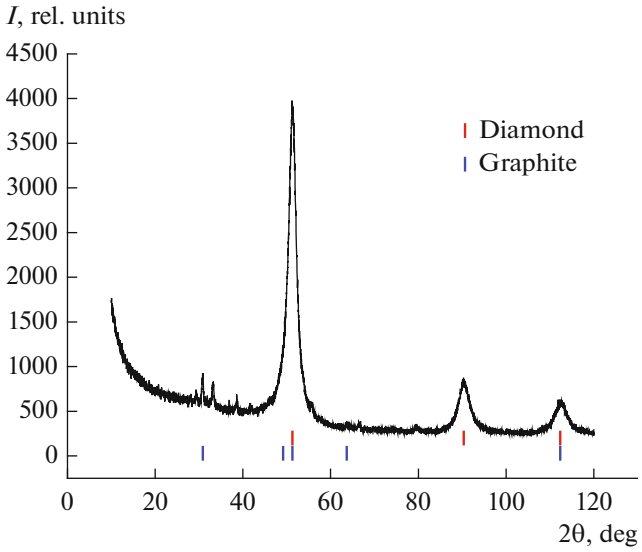

Fig. A1. X-ray diffraction pattern of DND powder.

Table A1. Some parameters of the total dependence of the pair interaction energy on the interparticle distance for DND particles (6.3 nm), with the parameters being calculated according to the extended DLVO theory, and aggregation factors at natural pH. $A = 1.38 \times 10^{-19}$ J

C, M	Parameters V_s		V_{max}/kT	h_{max}, nm	$-V_{min}/kT$	h_{min}, nm	W_1	W_2	ζ^w, mV
	$K \times 10^6$, J/m^3	l, nm							
5×10^{-4}	0	–	1.2	8.1	0.01	96.8	4.5	96.90	37.2
1×10^{-3}			0.87	7.15	0.03	57.4	3.35	38.9	37.5
2.5×10^{-3}			0.24	6.8	0.09	26.7	2.1	11.85	36.5
3×10^{-3}			0.06	7.2	0.12	21.9	1.8	9.1	35.2
5×10^{-3}			Attraction at all distances				1		30.9
1×10^{-2}									24.8
3×10^{-2}									14.5
1×10^{-3}	1	1	0.87	7.15	0.03	57.4	3.5	38.9	37.5
2.5×10^{-3}			0.25	6.7	0.09	26.7	2.2	11.8	36.5
3×10^{-3}			0.065	7.1	0.12	21.9	1.9	9.1	35.2
5×10^{-3}			Attraction at all distances				1		30.9
1×10^{-2}									24.8
3×10^{-2}									14.5

Table A2. Some parameters of the total dependence of the pair interaction energy on the interparticle distance for DND particles (45 nm), with the parameters being calculated according to the extended DLVO theory, and aggregation factors at natural pH. $A = 1.38 \times 10^{-19}$ J

C, M	Parameters V_s		V_{max}/kT	h_{max}, nm	$-V_{min}/kT$	h_{min}, nm	W_1	W_2	ζ^w, mV
	$K \times 10^6$, J/m^3	l, nm							
5×10^{-4}	1	1	8.8	7.9	0.07	96.6	2.7×10^3	14.09	37.2
1×10^{-3}			6.2	7.1	0.18	57.4	214	5.9	37.5
2.5×10^{-4}			1.8	6.7	0.63	26.7	3.9	2.1	36.5
3×10^{-3}			0.46	6.8	0.8	21.9	1.9	1.8	35.2
5×10^{-3}			Attraction at all distances				1	1	30.9
1×10^{-2}							1	1	24.8
3×10^{-2}							1	1	14.5
5×10^{-4}	0	–	8.7	8.1	0.07	96.8	2.7×10^3	14.0	37.2
1×10^{-3}			6.2	7.1	0.18	57.4	206	5.9	37.5
2.5×10^{-4}			1.75	6.8	0.63	26.7	3.8	2.1	36.5
3×10^{-3}			0.45	7.2	0.83	21.9	1.9	1.8	35.2
5×10^{-3}			Attraction at all distances				1	1	30.9
1×10^{-2}							1	1	24.8
5×10^{-4}	1	2	17.7	2.29	0.07	96.8	$>10^7$	14	37.2
1×10^{-3}			16.95	2.2	0.18	57.4	$>10^6$	5.9	37.5
3×10^{-3}			12.5	2.1	0.8	21.9	5.1×10^4	1.8	35.2
5×10^{-3}			9.1	2.2	1.0	18.6	1.8×10^3	1.6	30.9
1×10^{-2}			4.3	2.2	2.3	9.7	17.3	1.1	24.8

Table A3. Some parameters of the total dependence of the pair interaction energy on the interparticle distance for DND particles (135 nm), with the parameters being calculated according to the extended DLVO theory, and aggregation factors at natural pH. $A = 1.38 \times 10^{-19}$ J

C, M	Parameters V_s		V_{max}/kT	h_{max}, nm	$-V_{min}/kT$	h_{min}, nm	W_1	W_2	ζ^w, mV
	$K \times 10^6$, J/m^3	l, nm							
5×10^{-4}	0	–	26.36	8.1	0.22	968	$>10^{10}$	5.0	37.2
1×10^{-3}			18.6	7.1	0.56	57.4	$>10^7$	2.3	37.5
2.5×10^{-3}			5.25	6.8	1.9	26.7	32.8	1.18	36.5
3×10^{-3}			1.35	7.2	2.5	21.9	1.8	1.09	35.2
5×10^{-3}			Attraction at all distances				1	1	30.9
1×10^{-2}							1	1	24.8
3×10^{-2}							1	1	14.5
5×10^{-4}	1	1	26.36	7.9	0.22	96.8	$>10^{10}$	5.0	37.2
1×10^{-3}			18.65	7.1	0.56	57.4	$>10^7$	2.3	37.5
2.5×10^{-3}			5.3	6.7	1.9	26.7	35.6	1.2	36.5
3×10^{-3}			1.4	7.1	2.5	21.9	1.8	1.09	35.2
5×10^{-3}			Attraction at all distances				1	1	30.9
5×10^{-4}	1	2	53.1	2.2	0.2	96.8	$>10^{10}$	5.0	30.9
5×10^{-3}	1	2	24.22	2.1	5.2	12.3	$>10^9$	1.0	30.9
5×10^{-3}	1	3	206.42	1.3	3.5	20.0	$>10^8$	1.03	30.9
1×10^{-2}	1	1	Attraction at all distances						24.8
1×10^{-2}	1	2	9.3	2.2	10	8.3	925	1	24.8
3×10^{-2}	1	2	Attraction at all distances				1	1	14.5

Table A4. Some parameters of the total dependence of the pair interaction energy on the interparticle distance for DND particles (45 nm), with the parameters being calculated according to the extended DLVO theory, and aggregation factors at natural pH. $A_{eff} = 0.86 \times 10^{-19}$ J

C, M	Parameters V_s		V_{max}/kT	h_{max}, nm	$-V_{min}/kT$	h_{min}, nm	W_1	W_2	ζ^w, mV
	$K \times 10^6$, J/m^3	l, nm							
5×10^{-4}	0	–	11.2	6.1	0.04	196.8	2.8×10^4	26.09	37.2
1×10^{-3}			9.1	5.3	0.1	65.3	3.2×10^3	11	37.5
2.5×10^{-3}			4.4	4.9	0.3	32.1	31.1	3.7	36.5
3×10^{-3}			3.3	4.9	0.4	27.6	13.8	3.0	35.2
5×10^{-3}			Attraction at all distances				1	1	30.9
1×10^{-2}							1	1	24.8
5×10^{-4}	1	1	11.3	6.1	0.04	106.8	3.0×10^4	26	37.2
1×10^{-3}			9.2	5.1	0.09	65.3	3.7×10^3	11	37.5
2.5×10^{-3}			5.2	4.4	0.31	32,.8	$>10^{10}$	3.8	36.5
3×10^{-3}			3.7	4.5	0.4	27.6	16.9	3.0	35.2
5×10^{-3}			0.02	5.6	0.8	16.7	1.6	1.8	30.9
1×10^{-2}			Attraction at all distances				1	1	24.8
5×10^{-4}	1	2	29.7	1.5	0.04	106.8	$>10^{11}$	26.0	37.2
1×10^{-3}			29.3	1.4	0.09	65.3	$>10^{11}$	11.0	37.5
2.5×10^{-3}			25.9	1.4	0.31	32.7	$>10^{10}$	3.8	36.5
3×10^{-3}			25.3	1.4	0.4	27.7	$>10^{10}$	3.0	35.2
5×10^{-3}			20.8	1.4	0.8	17.2	1.5×10^8	1.8	30.9
1×10^{-2}			15.6	1.4	1.6	10.8	8.8×10^5	1.25	24.8

Table A5. Some parameters of the total dependence of the pair interaction energy on the interparticle distance for DND particles (135 nm) at a natural pH, with the parameters being calculated according to the extended DLVO theory. $A_{eff} = 0.86 \times 1\,0^{-19}$ J

C, M	Parameters V_s		V_{max}/kT	h_{max}, nm	$-V_{min}/kT$	h_{min}, nm	W_1	W_2	ζ^w, mV
	$K \times 10^6$, J/m^3	l, nm							
5×10^{-4}	0	–	33.7	6.1	0.12	106.8	$>10^{13}$	9.0	37.2
1×10^{-3}			27.4	5.3	0.28	56.3	$>10^{11}$	4.0	37.5
2.5×10^{-3}			15.0	4.8	0.92	32.8	4.1×10^3	1.7	36.5
3×10^{-3}			10.6	4.9	1.2	27.6	5.4×10^3	1.4	35.2
5×10^{-3}			Attraction at all distances				1	1	30.9
1×10^{-2}							1	1	24.8
3×10^{-2}							1	1	14.5
5×10^{-4}	1	1	33.8	6.1	0.12	106.8	$>10^{13}$	9.0	37.2
1×10^{-3}			27.7	5.1	0.29	65.3.3	$>10^{11}$	4.0	37.5
2.5×10^{-3}			15.2	4.4	0.92	32.8	7.6×10^3	1.7	36.5
3×10^{-3}			11.4	4.5	1.2	27.6	935	1.4	35.2
5×10^{-3}			0.08	5.6	2.4	16.7	1.25	1.1	30.9
5×10^{-3}	1	2	62.4	1.4	2.4	17.2	$>10^{10}$	1.1	30.9
5×10^{-3}	1	3	265.4	1.0	1.8	22.6	$>10^{10}$	1.2	30.9
1×10^{-2}	1	1	Attraction at all distances				1		24.8

Table A6. Some parameters of the total dependence of the pair interaction energy of DND particles (45 nm) on the interparticle distance, calculated using the extended DLVO theory, and aggregation factors at natural pH values. $A_{eff} = 0.58 \times 10^{-19}$ J

C, M	Parameters V_s		V_{max}/kT	h_{max}, nm	$-V_{min}/kT$	h_{min}, nm	W_1	W_2	ζ^W, mV
	$K \times 10^6$, J/m^3	l, nm							
5×10^{-4}	1	1	13.2	4.7	0.02	115.5	2.1×10^5	43.99	37.2
1×10^{-3}			11.6	3.6	0.06	71.73	4×10^4	18.6	37.5
2.5×10^{-3}			8.2	2.9	0.17	36.2	1.1×10^3	6.3	36.5
3×10^{-3}			6.6	3.0	0.22	31.8	245	5.0	35.2
5×10^{-3}			2.4	3.4	0.44	20.3	5.7	2.8	30.9
1×10^{-2}			Attraction at all distances				1		24.8
3×10^{-2}									14.5
5×10^{-4}	0	–	13.1	4.9	0.02	115.5	1.6×10^5	43.9	37.2
1×10^{-3}			11.3	4.2	0.06	71.7	2.5×10^4	18.6	37.5
2.5×10^{-3}			7.2	3.7	0.17	36.8	190	6.3	36.5
3×10^{-3}			6.0	3.75	0.23	31.8	124	5.0	35.2
5×10^{-3}			2.0	4.2	0.44	20.3	3.9	2.8	30.9
1×10^{-2}			Attraction at all distances				1		24.8
3×10^{-2}									14.5
1×10^{-3}	1	2	38.5	1.1	0.06	71.4	5.6×10^{15}	18.6	37.5
2.5×10^{-3}			36.7	1.1	0.17	37,.2	10^{15}	6.3	36.5
3×10^{-3}			35.1	1.1	0.2	31.9	1×10^{14}	5.0	35.2
5×10^{-3}			30.6	1.1	0.43	20.5	2.4×10^{12}	2.8	30.9
1×10^{-2}			25.2	1.1	0.9	25	1.1×10^{10}	1.7	24.8
3×10^{-2}			19.5	1.1	2.3	10.1	3.9×10^7	1.4	14.5
5×10^{-4}	1	1.25	14.3	2.6	0.02	115.5	6.5×10^5	43.9	37.2
1×10^{-3}			13.4	2.2	0.06	71.7.	2.1×10^5	18.6	37.5
2.5×10^{-3}			11.2	1.9	0.17	37.5	1.8×10^4	6.4	36.5
3×10^{-3}			6.6	3.0	0.22	31.8	245	5.0	35.2
5×10^{-3}			2.4	3.4	0.44	20.3	5.7	2.8	30.9
1×10^{-2}			Attraction at all distances				1		24.8

Table A7. Some parameters of the total dependence of the pair interaction energy on the interparticle distance for DND particles (135 nm), with the parameters being calculated according to the extended DLVO theory, and aggregation factors at natural pH values. $A_{eff} = 0.58 \times 10^{-19}$ J

C, M	Parameters V_s		V_{max}/kT	h_{max}, nm	$-V_{min}/kT$	h_{min}, nm	W_1	W_2	ζ^W, mV
	$K \times 10^6$, J/m^3	l, nm							
5×10^{-4}	1	1	39.7	4.5	0.07	115.5	2.5×10^{16}	15.09	37.2
1×10^{-3}			35.0	3.6	0.16	71.7	2.1×10^{14}	6.6	37.5
2.5×10^{-3}			24.5	2.9	0.52	37.2	5.4×10^{9}	2.5	36.5
3×10^{-3}			19.8	3.0	0.66	31.8	5.3×10^{7}	2.1	35.2
5×10^{-3}			7.34	3.4	1.3	20.3	240	1.37	30.9
1×10^{-2}			Attract× ion at all distances				1		24.8
3×10^{-2}									14.5
5×10^{-4}	0	1	39.2	4.9	0.07	115.5	1.4×10^{16}	15.09	37.2
1×10^{-3}			34.0	4.2	0.17	71.7	6.5×10^{13}	6.55	37.5
2.5×10^{-3}			22.6	3.7	0.52	37.2	7.4×10^{8}	2.5	36.5
3×10^{-3}			18	3.7	0.7	31.8	7.9×10^{6}	2.06	35.2
5×10^{-3}			6.2	4.2	1.3	20.3	67	1.37	30.9
1×10^{-2}			Attraction at all distances				1		24.8
3×10^{-2}									14.5
5×10^{-4}	1	2	116.3	1.3	0.07	115.5	$>10^{48}$	15.09	37.2
1×10^{-3}			116.5	1.1	0.165	71.7	$>10^{48}$	6.55	37.5
2.5×10^{-3}			110.1	1.07	0.52	37.2	$>10^{46}$	2.5	36.5
3×10^{-3}			105.4	1.08	0.66	31.9	$>10^{44}$	2.06	35.2
5×10^{-3}			91.7	1.1	1.3	20.5	$>10^{38}$	1.37	30.9T
1×10^{-2}			75.7	1.1	3.8	10.1	$>10^{31}$	1.07	24.8
5×10^{-4}	1	1.25	43.0	2.5	0.07	115.5	7×10^{17}	15.0	37.2
1×10^{-3}			40.3	2.2	0.16	71.7	4×10^{16}	6.6	37.5
2.5×10^{-3}			31.7	1.9	0.52	37.2	6.3×10^{12}	2.5	36.5
3×10^{-3}			27.18	1.9	0.66	31.8	5.8×10^{10}	2.06	35.2
5×10^{-3}			13.84	2	1.3	20.2	1.1×10^{5}	1.37	30.9
1×10^{-2}			Attraction at all distances				1		24.8
3×10^{-2}									14.5

ACKNOWLEDGMENTS

The authors are grateful to D.A. Aleksandrov for the measurements of the specific surface area. The study was carried out using the equipment of the Interdisciplinary Resource Centre for Nanotechnology, the Centre for Optical and Laser Materials Research, the Centre for Physical Methods of Surface Investigation, and the Centre for X-ray Diffraction Studies at the Research Park of St. Petersburg State University.

FUNDING

The work was supported by the Russian Science Foundation, project no. 23-23-00333.

CONFLICT OF INTEREST

The authors of this work declare that they have no conflicts of interest.

REFERENCES

1. Rosenholm, J.M., Vlasov, I.I., Burikov, S.A., et al., Nanodiamond-based composite structures for biomedical imaging and drug delivery, *J. Nanosci. Nanotechnol.*, 2015, vol. 15, no. 2, pp. 959–971. https://doi.org/10.1166/jnn.2015.9742
2. Schrand, A.M., Hens, S.A.C., and Shenderova, O.A., Nanodiamond particles: Properties and perspectives for bioapplications, *Crit. Rev. Solid State Mater. Sci.*, 2009, vol. 34, nos. 1–2, pp. 18–74. https://doi.org/10.1080/10408430902831987
3. Turcheniuk, K. and Mochalin, V.N., Biomedical applications of nanodiamond, *Nanotechnology*, 2017, vol. 28, pp. 252001–252027. https://doi.org/10.1016/j.slast.2023.03.007
4. Yu, Y., Nishikawa, M., Liu, M., et al., Self-assembled nanodiamond supraparticles for anticancer chemotherapy, *Nanoscale*, 2018, vol. 10, no. 19, pp. 8969–8978. https://doi.org/10.1039/C8NR00641E
5. Qin, S.-R., Zhao, Q., Cheng, Z.-G., et al., Rare earth-functionalized nanodiamonds for dual-modal imaging and drug delivery, *Diamond Relat. Mater.*, 2019, vol. 91, pp. 173–182. https://doi.org/10.1016/j.diamond.2018.11.015
6. Alkahtani, M.H., Alghannam, F., Jiang, L., et al., Fluorescent nanodiamonds: Past, present, and future, *Nanophotonics*, 2018, vol. 7, no. 8, pp. 1423–1453. https://doi.org/10.1515/nanoph-2018-0025
7. Nunn, N., d'Amora, M., Prabhakar, N., et al., Fluorescent single-digit detonation nanodiamond for biomedical applications, *Methods Appl. Fluoresc.*, 2018, vol. 6, no. 3, p. 035010. https://doi.org/10.1088/2050-6120/aac0c8
8. Panich, A.M., Salti, M., Prager, O., et al., PVP-coated Gd-grafted nanodiamonds as a novel and potentially safer contrast agent for in vivo MRI, *Magn. Reson. Med.*, 2021, vol. 86, no. 2, pp. 935–942. https://doi.org/10.1002/mrm.28762
9. Panich, A.M., Salti, M., Goren, S.D., et al., Gd(III)-grafted detonation nanodiamonds for MRI contrast enhancement, *J. Phys. Chem. C*, 2019, vol. 123, no. 4, pp. 2627–2631. https://doi.org/10.1021/acs.jpcc.8b11655
10. Panich, A.M., Shames, A.I., Goren, S.D., et al., Examining relaxivities in suspensions of nanodiamonds grafted by magnetic entities: Comparison of two approaches, *Magn. Reson. Mater. Phys., Biol. Med.*, 2020, vol. 33, pp. 885–888. https://doi.org/10.1007/s10334-020-00847-3
11. Panich, A.M., Shames, A.I., Aleksenskii, A.E., et al., Manganese-grafted detonation nanodiamond, a novel potential MRI contrast agent, *Diamond Relat. Mater.*, 2021, vol. 119, p. 108590. https://doi.org/10.1016/j.diamond.2021.108590
12. Fujisaku, T., Tanabe, R., Onoda, S., et al., pH nanosensor using electronic spins in diamond, *ACS Nano*, 2019, vol. 13, no. 10, pp. 11726–11732. https://doi.org/10.1021/acsnano.9b05342
13. Batsanov, S.S., Dan'kin, D.A., Gavrilkin, S.M., et al., Structural changes in colloid solutions of nanodiamond, *New J. Chem.*, 2020, vol. 44, no. 4, pp. 1640–1647. https://doi.org/10.1039/C9NJ05191K
14. Mchedlov-Petrossyan, N.O., Kamneva, N.N., Marynin, A.I., et al., Colloidal properties and behaviors of 3 nm primary particles of detonation nanodiamonds in aqueous media, *Phys. Chem. Chem. Phys.*, 2015, vol. 17, no. 24, pp. 16186–16203. https://doi.org/10.1039/C5CP01405K
15. Mchedlov-Petrossyan, N.O., Kamneva, N.N., Kryshtal, A.P., et al., The properties of 3 nm-sized detonation diamond from the point of view of colloid science, *Ukr. J. Phys.*, 2015, vol. 60, no. 9, pp. 932–937. https://doi.org/10.15407/ujpe60.09.0932
16. Mchedlov-Petrossyan, N.O., Kriklya, N.N., Kryshtal, A.P., et al., The interaction of the colloidal species in hydrosols of nanodiamond with inorganic and organic electrolytes, *J. Mol. Liq.*, 2019, vol. 283, pp. 849–859. https://doi.org/10.1016/j.molliq.2019.03.095
17. Kamneva, N.N., Tkachenko, V.V., Mchedlov-Petrossyan, N.O., et al., Interfacial electrical properties of nanodiamond colloidal species in aqueous medium as examined by acid-base indicator dyes, *Surface Engineering and Applied Electrochemistry*, 2018, vol. 54, pp. 64–72. https://doi.org/10.3103/S1068375518010088
18. Korobov, M.V., Avramenko, N.V., and Bogachev, A.G., Nanophase of water in nano-diamond gel, *J. Phys. Chem.*, 2007, vol. 111, no. 20, pp. 7330–7334. https://doi.org/10.1021/jp0683420
19. Batsanov, S.S., Lesnikov, E.V., Dan'kin, D.A., and Balakhanov, D.M., Water shells of diamond nanoparticles in colloidal solutions, *Appl. Phys. Lett.*, 2014, vol. 104, no. 13, p. 133105. https://doi.org/10.1063/1.4870464
20. Petit, T., Puskar, L., Dolenko, T., et al., Unusual water hydrogen bond network around hydrogenated nanodiamonds, *J. Phys. Chem.*, 2017, vol. 121, no. 9, pp. 5185–5194. https://doi.org/10.1021/acs.jpcc.7b00721
21. Petit, T., Yuzawa, H., Nagasaka, M., et al., Probing interfacial water on nanodiamonds in colloidal dispersion, *J. Phys. Chem. Lett.*, 2015, vol. 6, no. 15, pp. 2909–2912. https://doi.org/10.1021/acs.jpclett.5b00820

22. Emelyanenko, A.M., Emelyanenko, K.A., Vul, A.Ya., et al., The role of nanoparticle charge in crystallization kinetics and ice adhesion strength for dispersionsof detonation nanodiamonds, *Phys. Chem. Chem. Phys.*, 2023, vol. 25, no. 5, pp. 3950–3958. https://doi.org/10.1039/D2CP05144C
23. Batsanov, S.S., Gavrilkin, S.M., Korzhenevskiy, A.P., et al., Giant permittivity of confined water on nanodiamonds, *J. Phys. Chem. C*, 2022, vol. 126, no. 14, pp. 6385–6393. https://doi.org/10.1021/acs.jpcc.1c08827
24. Chiganova, G.A., The effect of particle hydration on the aggregation stability of ultradispersed diamond hydrosols, *Colloid J.*, 1997, vol. 59, no. 1, pp. 87–89.
25. Chiganova, G.A., Aggregation of particles in ultradispersed diamond hydrosols, *Colloid J.*, 2000, vol. 62, no. 2, pp. 238–243.
26. Moraru, V.N., Ovcharenko, F.D., and Trotskaya, L.A., Stability and electro-surface properties of the water dispersions of the oxidized synthetic diamond, *Kolloidn. Zh.*, 1991, vol. 53, no. 5, pp. 874–879.
27. Ovcharenko, A.G., Solokhina, A.B., Sataev, R.R., and Ignatenko, A.V., Electrophoretic behavior of ultrafine diamond particle aggregates, *Kolloidn. Zh.*, 1991, vol. 53, no. 6, pp. 1067–1071.
28. Chiganova, G.A. and Gosudareva, E.Yu., Structure formation in aqueous dispersions of detonation nanodiamonds, *Nanotechnol. Russ.*, 2016, vol. 11, nos. 7–8, pp. 401–406. https://doi.org/10.1134/S1995078016040042
29. Sychev, D.Y., Zhukov, A.N., Golikova, E.V., and Sukhodolov, N.G., The effect of simple electrolytes on coagulation of hydrosols of monodisperse negatively charged detonation nanodiamond, *Colloid J.*, 2017, vol. 79, no. 6, pp. 822–828. https://doi.org/10.1134/S1061933X17060163
30. Mchedlov-Petrossyan, N.O., Kriklya, N.N., Laguta, A.N., and Osawa, E., Stability of detonation nanodiamond colloid with respect to inorganic electrolytes and anionic surfactants and solvation of the particles surface in DMSO–H_2O organo-hydrosols, *Liquids*, 2022, vol. 2, no. 3, pp. 196–209. https://doi.org/10.3390/liquids2030013
31. Volkova, A.V., Vdovichenko, D.A., Golikova, E.V., and Ermakova, L.E., The regularities of coagulation in polydisperse zirconia nanosol, *Colloid J.*, 2021, vol. 83, no. 5, pp. 546–557. https://doi.org/10.1134/S1061933X21050136
32. Wiersema, P.H., Loeb, A.L., and Overbeek, J.T.G., Calculation of the electrophoretic mobility of a spherical colloid particle, *J. Colloid Interface Sci.*, 1966, vol. 22, no. 1, pp. 78–99. https://doi.org/10.1016/0021-9797(66)90069-5
33. Derjaguin, B.V. and Landau, L.D., Theory of the stability of strongly charged lyophobic sols and of the adhesion of strongly charged particles in solutions of electrolytes, *Acta Physicochim. URSS*, 1941, vol. 14, no. 6, pp. 633–662.
34. Derjaguin, B. and Landau, L., Theory of the stability of strongly charged lyophobic sols and of the adhesion of strongly charged particles in solutions of electrolyte, *Prog. Surf. Sci.*, 1993, vol. 43, nos. 1–4, pp. 30–59. https://doi.org/10.1016/0079-6816(93)90013-L
35. Derjaguin, B.V., *Teoriya ustoichivosti kolloidov i tonkikh plenok* (Theory of Stability of Colloids and Thin Films), Moscow: Nauka, 1986.
36. Derjaguin, B.V. and Churaev, N.V., Inclusion of structural forces in the theory of stability of colloids and films, *J. Colloid Interface Sci.*, 1985, vol. 103, no. 2, pp. 542–553. https://doi.org/10.1016/0021-9797(85)90129-8
37. Boström, M., Deniz, V., Franks, G.V., and Ninham, B.W., Extended DLVO theory: Electrostatic and non-electrostatic forces in oxide suspensions, *Adv. Colloid. Interf. Sci.*, 2006, vols. 123–126, pp. 5–15. https://doi.org/10.1016/j.cis.2006.05.001
38. Churaev, N.V. and Sobolev, V.D., Contribution of structural forces to wetting of quartz surface by electrolyte solutions, *Colloid J.*, 2000, vol. 62, no. 2, pp. 244–250.
39. Oshima, H.J., Healy, T.W., and White, L.R., Improvement on Hogg–Healy–Fuerstenau formulas for the interaction on dissimilar double layers, *J. Colloid Interf. Sci.*, 1982, vol. 89, no. 2, pp. 484–493. https://doi.org/10.1016/0021-9797(82)90199-0
40. Casimir, H.B.G. and Polder, D., The influence of retardation on the London–van-der-Waals forces, *Phys. Rev.*, 1948, vol. 73, no. 4, pp. 360–372. https://doi.org/10.1103/PhysRev.73.360
41. Schenkel, J.H. and Kitchener, J.A., A test of the Derjaguin–Verwey–Overbeek theory with a colloidal suspension, *Trans. Faraday Soc.*, 1960, vol. 56, pp. 161–173. https://doi.org/10.1039/TF9605600161
42. Bergström, L., Hamaker constants of inorganic materials, *Adv. Colloid Interface Sci.*, 1997, vol. 70, pp. 125–169. https://doi.org/10.1016/S0001-8686(97)00003-1
43. Derjaguin, B.V., Churaev, N.V., and Muller, V.M., *Surface Forces*, New York: Consultants Bureau, 1987.
44. McGown, D.N.L. and Parfitt, G.D., Improved theoretical calculation of stability ratio for colloidal systems, *J. Phys. Chem.*, 1967, vol. 71, no. 2, pp. 419–450. https://doi.org/10.1021/j100861a041
45. Molina-Bolívar, J.A., Galisteo-González, F., and Hidalgo-Álvarez R., Colloidal aggregation in energy minima of restricted depth, *J. Chem. Phys.*, 1999, vol. 110, no. 11, pp. 5412–5420. https://doi.org/10.1063/1.478436
46. Ruckenstein, E. and Huang, H., Colloid restabilization at high electrolyte concentrations: Effect of ion valency, *Langmuir*, 2003, vol. 19, no. 7, pp. 3049–3055. https://doi.org/10.1021/la026729y
47. Hogg, R. and Yang, K.C., Secondary coagulation, *J. Colloid Interface Sci.*, 1976, vol. 56, no. 3, pp. 573–576. https://doi.org/10.1016/0021-9797(76)90123-5
48. Petit, T. and Puskar, L., FTIR spectroscopy of nanodiamonds: Methods and interpretation, *Diamond Relat. Mater.*, 2018, vol. 89, pp. 52–66. https://doi.org/10.1016/j.diamond.2018.08.005
49. Shenderova, O., Panich, A.M., Moseenkov, S., et al., Hydroxylated detonation nanodiamond: FTIR, XPS, and NMR studies, *Phys. Chem. C*, 2011, vol. 115, no. 39, pp. 19005–19011. https://doi.org/10.1021/jp205389m
50. Kulakova, I.I., Nanodiamond surface chemistry, *Fiz. Tverd. Tela*, 2004, vol. 46, no. 4, pp. 621–628.
51. Mochalin, V., Osswald, S., and Gogotsi, Yu., Contribution of functional groups to the Raman spectrum of

nanodiamond powders, *Chem. Mater.*, 2009, vol. 21, no. 2, pp. 273–279. https://doi.org/10.1021/cm802057q

52. Sharin, P.P., Sivtseva, A.V., Yakovleva, S.P., et al., Comparison of morphological and structural characteristics of nanopowder particles obtained by natural diamond grinding and detonation synthesis, *Izv. VUZov, Poroshk. Metall. Funkts. Pokrytiya*, 2019, no. 4, pp. 55–67. https://doi.org/10.17073/1997-308X-2019-4-55-67
53. Sharin, P.P., Sivtseva, A.V., and Popov, V.I., Air-thermal oxidation of diamond nanopowders obtained by the methods of mechanical grinding and detonation synthesis, *Izv. VUZov, Poroshk. Metall. Funkts. Pokrytiya*, 2022, no. 4, pp. 67–83. https://doi.org/10.17073/1997-308X-2022-4-67-83
54. Sharin, P.P., Sivtseva, A.V., and Popov, V.I., X-ray photoelectron spectroscopy of nanodiamonds obtained by grinding and detonation synthesis, *Tech. Phys.*, 2021, vol. 66, pp. 275–279. https://doi.org/10.1134/S1063784221020183
55. Thomas, A., Parvathy, M.S., and Jinesh, K.B., Synthesis of nanodiamonds using liquid-phase laser ablation of graphene and its application in resistive random access memory, *Carbon Trends*, 2021, vol. 3, p. 100023. https://doi.org/10.1016/j.cartre.2020.100023
56. Lim, D.G., Kim, K.H., Kang, E., et al., Comprehensive evaluation of carboxylated nanodiamond as a topical drug delivery system, *Int. J. Nanomed.*, 2016, vol. 11, pp. 2381–2395. https://doi.org/10.2147/IJN.S104859
57. Frese, N., Mitchell, S.T., Bowers, A., et al., Diamond-like carbon nanofoam from low-temperature hydrothermal carbonization of a sucrose/naphthalene precursor solution, *Journal of Carbon Research*, 2017, vol. 3, no. 3, p. 23. https://doi.org/10.3390/c3030023
58. Testolin, A., Cattaneo, S., Wang, W., et al., Cyclic Voltammetry characterization of Au, Pd, and AuPd nanoparticles supported on different carbon nanofibers, *Surfaces*, 2019, vol. 2, no. 1, pp. 205–215. https://doi.org/10.3390/surfaces2010016